



# The influence of variations in crustal composition and lithospheric strength on the evolution of deformation processes in the southern Central Andes: insights from geodynamic models

Matías Barrionuevo<sup>1</sup> · Sibiao Liu<sup>2,4</sup> · José Mescua<sup>1</sup> · Daniel Yagupsky<sup>3</sup> · Javier Quinteros<sup>2</sup> · Laura Giambiagi<sup>1</sup> · Stephan V. Sobolev<sup>2,4</sup> · Constanza Rodríguez Picada<sup>2,4</sup> · Manfred R. Strecker<sup>4</sup>

Received: 22 April 2020 / Accepted: 5 January 2021 / Published online: 11 February 2021  
© Geologische Vereinigung e.V. (GV) 2021

## Abstract

Deformation in the orogen-foreland system of the southern Central Andes between 33° and 36° S varies in style, locus, and amount of shortening. The controls that determine these spatially variable characteristics have largely remained unknown, yet both the subduction of the oceanic Nazca plate and the strength of the South American plate have been invoked to play a major role. While the parameters governing the subduction processes are similar between 33° and 36° S, the lithospheric strength of the upper plate is spatially variable due to structures inherited from past geodynamic regimes and associated compositional differences in the South American plate. Regional Mesozoic crustal horizontal extension generated a < 40-km-thick crust with a more mafic composition in the lower crust south of 35°S; north of this latitude, however, a more felsic lower crust is inferred from geophysical data. To assess the influence of different structural and compositional heterogeneities on the style of deformation in the southern Central Andes, we developed a suite of geodynamic models of intraplate lithospheric shortening for two E–W transects (33° 40' S and 36° S) across the Andes. The models are constrained by local geological and geophysical information. Our results demonstrate a decoupled shortening mode between the brittle upper crust and the ductile lower crust in those areas characterized by a mafic lower crust (36° S transect). In contrast, a more felsic lower crust, such as in the 33° 40' S transect, results in a coupled shortening mode. Furthermore, we find that differences in lithospheric thickness and the asymmetry of the lithosphere–asthenosphere boundary may promote the formation of a crustal-scale, west-dipping detachment zone that drives the overall deformation and lateral expansion of the orogen. Our study represents the first geodynamic modeling effort in the southern Central Andes aimed at understanding the roles of heterogeneities (crustal composition and thickness) at the scale of the entire lithosphere as well as the geometry of the lithosphere–asthenosphere boundary with respect to mountain building.

**Keywords** Southern Central Andes · Coupled/decoupled deformation · Crustal composition · Lithospheric strength · Direction of tectonic transport

## Introduction

The southern Central Andes (27°–46° 30' S) at the western South American plate margin represent a typical subduction orogen that has developed from the Late Cretaceous to the present day (e.g., Jordan et al. 1983; Mpodozis and Ramos 1989; Ramos 1999; Hervé et al. 2000; Oncken et al. 2006). Terrane accretion in this geodynamic setting played an important role during the Paleozoic, which subsequently influenced the style of deformation during Mesozoic and Cenozoic non-collisional mountain building (Ramos et al. 1986; Mpodozis and Ramos 1989; Charrier et al. 2015). The Andean orogenic system exhibits major

✉ Matías Barrionuevo  
matbarrionuevo@yahoo.com.ar;  
mbarrionuevo@mendoza-conicet.gob.ar

<sup>1</sup> IANIGLA, CCT–Mendoza (CONICET), Mendoza, Argentina

<sup>2</sup> GFZ–German Research Center for Geosciences, Potsdam, Germany

<sup>3</sup> IDEAN, Instituto de Estudios Andinos “Don Pablo Groeber” (CONICET-Universidad de Buenos Aires), Buenos Aires, Argentina

<sup>4</sup> Institute for Geosciences, University of Potsdam, Potsdam, Germany

along-strike variations in the amount of shortening, topography, and style of deformation (Ramos et al. 1996; Kley et al. 1999; Oncken et al. 2006). The parameters that influence these along-strike variations can be classified into two main groups: (i) subduction-related parameters, i.e., slab dip, age of the subducting oceanic plate, bathymetric anomalies on the subducting Nazca plate, trench-fill thickness, and convergence obliquity (e.g., Jarrard 1986; Yáñez and Cembrano 2004; Sobolev and Babeyko 2005; Oncken et al. 2006); and (ii) upper-plate characteristics, such as the thermal state of the lithosphere, lithospheric strength variations due to different crustal and lithospheric thicknesses, and rheological heterogeneities (e.g., Allmendinger et al. 1983; Kley et al. 1999; Ramos et al. 2002; Pearson et al. 2013; Mouthereau et al. 2013; McGroder et al. 2015). The southern sector of this system, between 33° and 36° S, is affected by similar subduction parameters (i.e., a slab dip of ~30°; similar age of the oceanic plate; no major changes neither in plate-velocity vectors nor in climate; e.g., Cahill and Isacks 1992; Yáñez and Cembrano 2004; Somoza and Ghidella 2012; Strecker et al. 2007), but considerably differs in its tectonic history and, hence, in lithospheric composition and thickness of the upper plate.

In this study, we focus on this southern sector of the Central Andes to analyze the interplay between deformational styles and continental lithospheric characteristics (i.e., composition and thickness). We particularly explore the evolution of deformation along two segments across the southern Central Andes: a northern one between 33° and 35° S, and a southern one between 35° S and 36° S, represented by two cross sections at 33° 40' S and 36° S, respectively (Figs. 1, 2, 3). The cross-section portraying the northern segment is based on structural studies by Giambiagi et al. (2012, 2015), and the transect of the southern segment was constructed based on previously published partial cross sections (e.g., Giambiagi et al. 2012; Orts et al. 2012; Astaburuaga 2014; Tapia 2015) and our own field observations (Barrionuevo et al. 2019; Barrionuevo 2020). Both transects (Figs. 1, 2, 3) reveal important differences, in particular with respect to the locus and amount of shortening within the mountain range and the transition to the foreland. For example, 70 km of shortening has been estimated for the transect at 33° 40' S; while at 36° S, shortening amounts to approximately 45 km (Giambiagi et al. 2012, 2015). In the former, upper-crustal shortening is vertically aligned with the maximum crustal thickness and maximum topography; while in the latter, the location of upper-crustal shortening occurs farther east with

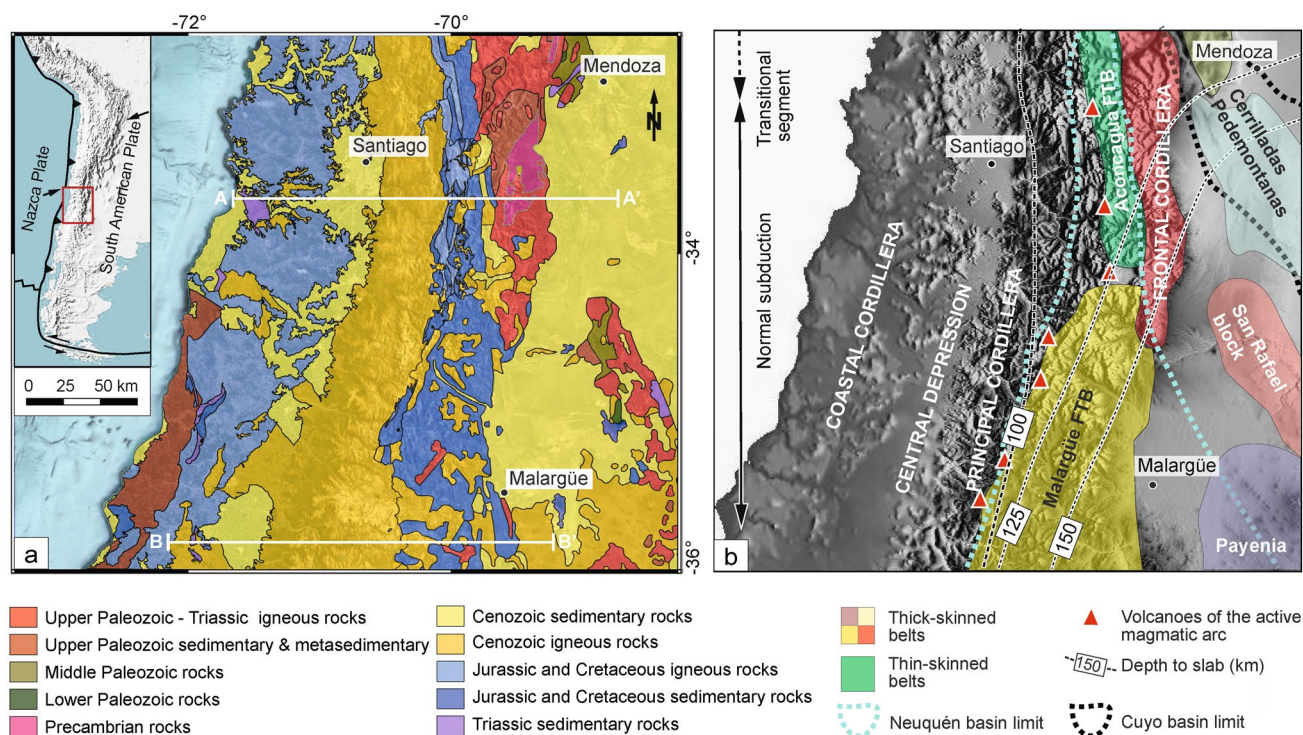


**Fig. 1** Location and characteristics of the study area. **a** Geological map of the study area, after SEGEMAR (1997), SERNAGEOMIN (2003) and Mescua et al. (2016). A–A' Location of the cross section at 33° 40' S. B–B' Location of the cross section at 36° S. **b** Principal morphotectonic provinces of the area, with the Aconcagua and

Malargüe fold-and-thrust belts (FTBs) and corresponding structural styles (thin- vs. thick-skinned deformation); the active magmatic arc and depth contours of the subducting Nazca plate (Cahill and Isacks 1992) are also shown

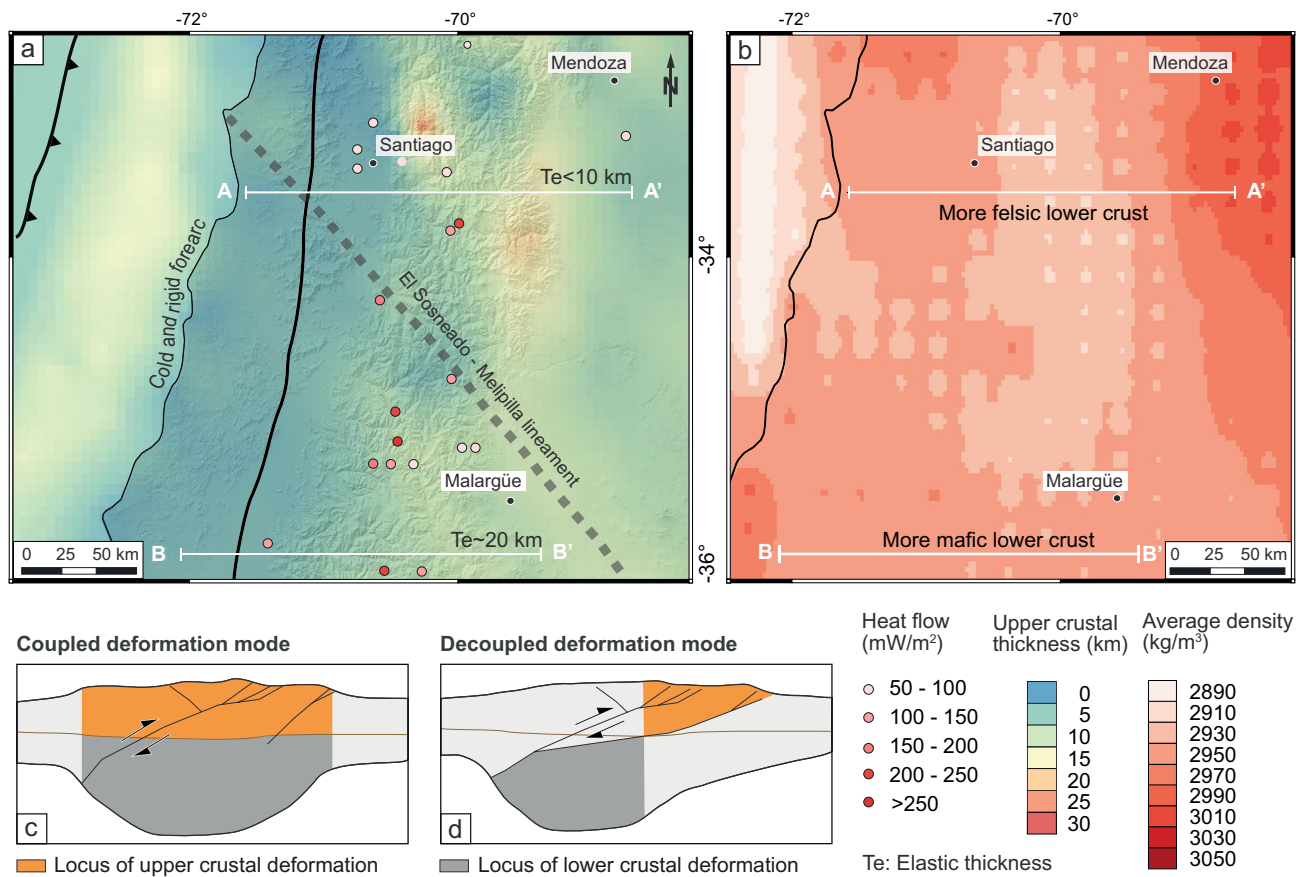


**Fig. 2** Geophysical features of the study area. **a** Heat flow and upper-crustal thickness of the study area. Individual heat-flow measurements based on Lucazeau (2019) and Rodríguez Picada (pers. comm. 2020). Due to the limited number of measurements, no contours are shown. Upper crustal thickness is based on Tassara and Echaurren 2012). Note that the thickness of felsic upper crust decreases southward, which contributes to a more mafic bulk composition of the crust for the southern transect (36° S). This corresponds with a greater elastic thickness ( $T_e$ ) according to Tassara and Yáñez (2003). **b** Average density (kg/m<sup>3</sup>) of the crust in the study area based on Rodríguez Picada et al. (2020) showing increasing values southward.

respect to the area where the maximum crustal thickness is located. Finally, regarding topographic differences between the two transects, the mean elevations are about 3400 m in the northern transect; whereas, they are about 2200 m in the southern transect (Giambiagi et al. 2012).

The variation of lithospheric strength of the upper plate in the study area is mainly influenced by pre-Cenozoic tectono-magmatic events (Uliana et al. 1989; Kleiman and Japas 2009; Giambiagi et al. 2012). A Triassic–Early Jurassic rifting phase thinned the crust south of 35° S (Sigismondi 2012), with a more mafic composition than in the northern counterpart, due to basaltic underplating (Kay et al. 1989; Llambías et al. 1993). Both factors—a thinner, yet underplated mafic sector in the south—would result in a stronger crust (Kusznir and Park 1986) compared with

In combination with the upper-crustal thickness and elastic thickness, the southern transect is characterized by a more mafic lower crust. **c** Cartoon showing the coupled deformation mode where upper- and lower-crustal shortening occur in the same vertical column of rocks. This corresponds to the “pure-shear” shortening or distributed crustal shortening mode (i.e., Allmendinger and Gubbels 1996). **d** Cartoon depicting the decoupled mode of deformation, where the loci of upper- and lower-crustal shortening are displaced laterally; this corresponds to the “simple-shear” deformation or discrete overthrusting of Allmendinger and Gubbels (1996), interpreted for the Andes of southern Bolivia and north-western Argentina

the crust in the northern transect (Figs. 2, 3). Further support for the notion of a significant compositional difference between both areas comes from the studies of Tassara and Yáñez (2003), based on estimations of elastic thickness ( $T_e$ ) of the Andean lithosphere. These authors recognized a southward-directed increase in elastic thickness (Fig. 2a) between 33.5° S and 39° S that is related to the transition between a quartz-dominated (i.e., more felsic) crust in the north to a plagioclase-dominated (i.e., more mafic) crust in the south. Importantly, a more mafic crust can result both in greater lithospheric strength (Kusznir and Park 1986) and a tendency to support a decoupled shortening mode (Fig. 2d), in which brittle-shortening processes in the upper crust are decoupled from the loci of viscous/ductile shortening in the lower crust (Allmendinger and Gubbels 1996). Conversely,

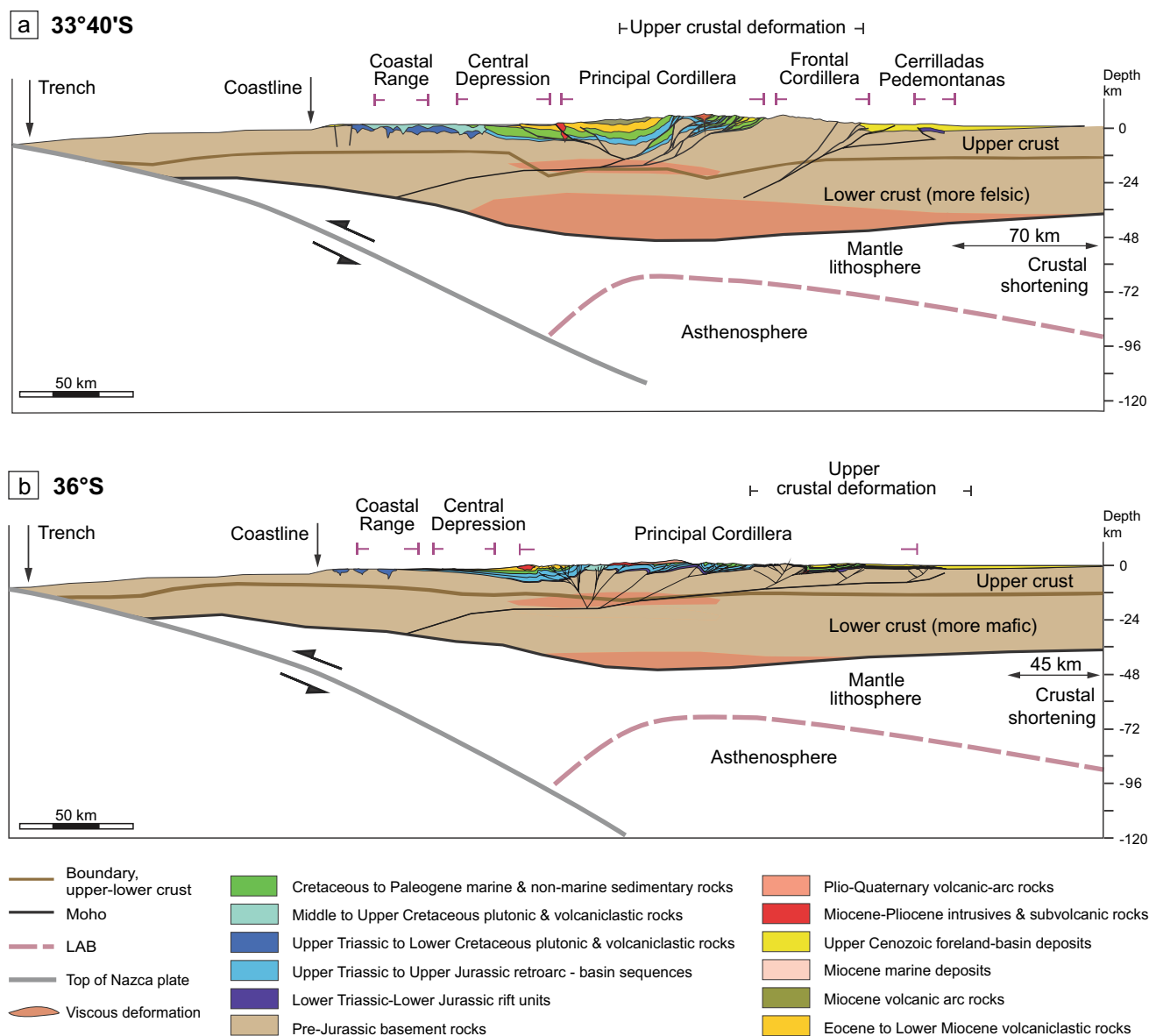


**Fig. 3** Cross sections along the two Andean transects. **a** Cross section at 33° 40' S (modified from Giambiagi et al. 2015). **b** Cross section at 36° S based on Giambiagi et al. (2012); Orts et al. (2012); Astaburuaga (2014); Tapia (2015); and our own data (Barrionuevo et al. 2019; Barrionuevo 2020). The major portion of shortening is accommodated within the eastern flanks of the Andes, here labeled as upper-crustal deformation. The boundary between upper and lower crust, the LAB (lithosphere–asthenosphere boundary), Moho, and

the geometry of Nazca slab are from Tassara and Echaurren (2012). The geological data are based on field surveys and depict the principal structures, the attitudes of bedding planes, and, where possible, fault-kinematic indicators. Where available, data from industry-style seismic reflection and oil-well data have been incorporated as well. The crustal and lithospheric geometries are based on geophysical data such as gravity anomalies and seismicity (Tassara and Echaurren 2012; Julve 2019)

the felsic composition north of 35° S would favor a coupled mode of deformation (Fig. 2c), in which upper brittle and lower viscous/ductile crustal deformation occurs in the same crustal column (Allmendinger and Gubbels 1996).

In addition to the different amount of shortening in the two transects, the northern and southern areas are said to exhibit coupled and decoupled styles, respectively (Giambiagi et al. 2012). Furthermore, the along-strike change in crustal

composition proposed for the study area may influence the thermal state of the orogen. Accordingly, a more felsic crust north of 35° S (e.g., Tassara and Yáñez 2003) would be associated with a higher concentration of radiogenic elements than its southern, more mafic counterpart. A more felsic crust contributes significantly to a higher heat budget of the lithosphere, which increases the temperature of the crust, thus weakening it. (e.g., Vilà et al. 2010). In contrast, when considering a crust

with more mafic components but similar thickness, temperatures are expected to be lower. As shown in Fig. 2a, heat-flow values along-strike of the orogen do not show a consistent decrease from the northern to the southern transect due to the limited data points; however, such a trend is visible at the larger, regional scale (Lucazeau 2019; Rodríguez Picada pers. comm. 2020). The greater heat budget in the northern area could, thus, affect the behavior of the already weaker, more felsic crust under deformation. An additional control of the thermal state of the lithosphere of the South American plate are subduction-related magmatic processes. However, since both areas are characterized by a similar style and duration of magmatism (Litvak et al. 2018), significant temperature variations between the two areas resulting from this process are negligible.

In addition to the influence of inherited structural and compositional heterogeneities on deformation characteristics in the upper plate, we address the direction of tectonic transport in the orogen, a topic that constitutes another subject of recent debate in Andean tectonic studies. The classical view of an orogen with dominantly east-directed structures (e.g., Ramos et al. 2004; Farías et al. 2010; Astini et al. 2010; Giambiagi et al. 2012; Turienzo et al. 2012; Buelow et al. 2018) has been recently challenged by a model that proposes west-directed transport, implying the existence of a deep-seated, east-dipping detachment that is thought to be responsible for westward-directed thrusting of the orogenic system over the rigid forearc block (Armijo et al. 2010; Riesner et al. 2018).

In this context, we aim to (i) analyze the role of variations in lithospheric strength (i.e., crustal composition and, crustal and lithospheric thickness) of the upper plate during the Cenozoic Andean orogenesis, and (ii) to discuss the conditions, such as lithospheric geometry of the upper plate, that may determine the direction of main tectonic transport in these areas of the southern Central Andes. To achieve this goal, we first briefly introduce the geological characteristics of the two transects and present the along-strike variation in deformation styles between them. Second, we develop geodynamic numerical models with different initial upper-plate configurations (i.e., different crustal composition and thickness) constrained by the available geophysical and geological data to investigate the influence of upper-plate characteristics (composition and thickness of crust and lithosphere) with respect to the Andean deformation style, including the direction of tectonic transport during the Cenozoic.

## Geological setting

### Pre-Andean history

The study area has been under the influence of protracted subduction since the Paleozoic, which resulted in several

periods of horizontal crustal shortening or horizontal extension (Ramos et al. 1986; Mpodozis and Ramos 1989; Azcuy and Caminos 1987; Astini et al. 1995; Massonne and Calderon 2008). The tectono-magmatic processes during these periods created crustal heterogeneities (i.e., changes in crustal composition and thickness, and zones of weakness such as faults and oriented fabrics) prior to the Late Cretaceous–Quaternary Andean orogeny, which influence the degree of lithospheric strength and lead to different structural styles in the study area.

Subsequent to the Early Permian horizontal shortening, widespread volcanism developed under horizontal extensional conditions from the Late Permian to the Early Triassic; the corresponding rocks of this episode are grouped into the Choiyoi Group (Upper Paleozoic–Triassic igneous rocks in Fig. 1; Llambías et al. 1993; Sato et al. 2015). The horizontal extensional conditions continued between the Early to Middle Triassic, with the formation of the continental Cuyo rift basin (Uliana et al. 1989).

During the Late Triassic to Early Jurassic, the Neuquén basin in the southern study area formed in a back-arc extensional setting, which was associated with a series of isolated depocenters that subsequently coalesced into larger sedimentary basins (Vergani et al. 1995). To the north of 35° S, these NNE- to NNW-trending depocenters contain early syn-rift deposits, more than ~2-km thick; while to the south, volcanic and volcanoclastic rocks as well as sedimentary sequences were deposited, accounting for more than ~4 km of thickness. The transition between a passive rift (north of 35° S) and an active rift (south of 35° S) spatially coincides with the Sosneado-Melipilla lineament (Fig. 2a), likely a Paleozoic crustal shear zone (Yáñez et al. 1998; Giambiagi et al. 2012; Piquer et al. 2020).

In the Late Cretaceous, the onset of Andean horizontal shortening, the accompanying build-up of topography, and concomitant erosion and deposition are recorded by coarse continental deposits in a foreland-basin setting (Vergani et al. 1995).

### Geological characteristics of the northern transect

Late Cretaceous tectonism in the transect along 33° 40' S was characterized by horizontal shortening and crustal thickening (Boyce et al. 2020), which generated a thicker crust (~40 km) in the westernmost zone of the transect where the Coastal Cordillera is located (Giambiagi et al. 2015).

The main Andean mountain building process in this segment started during the Miocene (20–18 Ma). Since that time, synorogenic deposits with volcanic and volcanoclastic intervals have been filling intermontane and foreland basins that record the Miocene–Quaternary Andean shortening and uplift (e.g., Irigoyen et al. 2000; Giambiagi et al. 2003b; Buelow et al. 2018). The volcanic

arc was located at that time along the western slope of the Principal Cordillera between 33° and 35° S. Subsequently, during Mio-Pliocene time, the arc migrated to the east to its current position where it coincides with the crest of the Andes (Stern and Skewes 1995).

According to trace-element patterns obtained from the Early to Middle Miocene tholeiitic rocks (Abanico Formation and stratigraphic equivalents), the crust was relatively thin (< 40 km) between 33° and 35° S (Nyström et al 2003; Kay et al. 2005), possibly due to horizontal extension during a geodynamic regime characterized by slab rollback (Charrier et al. 2002; Mpodozis and Cornejo 2012; Horton and Fuentes 2016). In contrast, from the Early Miocene onward (21–16 Ma), this region was instead characterized by horizontal shortening and, by the Pliocene, crustal thickness had increased to 50 km (e.g., Kay and Mpodozis 2002).

The northern segment (33°–35° S) includes the morphotectonic provinces of the Principal Cordillera and the Frontal Cordillera (Figs. 1, 3). The Aconcagua fold-and-thrust belt, within the Principal Cordillera morphotectonic province, has been interpreted as a thin-skinned fold-and-thrust belt in its northern sectors (e.g., Ramos 1988; Kozłowski et al. 1993; Ramos et al. 1996); to the south, however, reactivated, deep-seated Mesozoic basement structures have been involved in the deformation (Giambiagi et al. 2003a). The shortening estimates for this thrust belt are approximately 50 km at 33° 40' S (Giambiagi et al. 2015) and 23 km at 34° 40' S (Turienzo et al. 2012) in its eastern sector and including most of the eastern flanks of the Andes; while for the Western Principal Cordillera, less than 10 km of Miocene shortening has been estimated (Turienzo et al. 2012; Giambiagi et al. 2015). To the east, the Frontal Cordillera comprises a basement block that is associated with a limited amount of shortening of approximately 10 km (Giambiagi et al. 2012). The Frontal Cordillera ends abruptly south of 34° 40' S and it is covered by Cenozoic sediments. Farther east of the Frontal Cordillera, limited tectonic inversion of Mesozoic normal faults accounts for less than 5 km of shortening in the Cerrilladas Pedemontanas (Giambiagi et al. 2015). Total Miocene to present-day shortening for this transect is approximately 70 km, with varying shortening rates from 2 mm/year in the Early Miocene to 6.5 mm/year in the Middle Miocene (Giambiagi et al. 2015).

There is a marked decrease in the amount of shortening to the south of 34° 40' S; traditionally, this has been interpreted to be the direct result of the geodynamic boundary conditions, such as the angle of the subducting slab and the coupling between the upper and lower plates (e.g., Jordan et al. 1983; Ramos et al. 2004; Ramos 2010; Horton 2018).

## Geological characteristics of the southern transect

At 36° S, the onset of shortening is inferred to have started in the Late Cretaceous (Tunik et al. 2010; Mescua et al. 2013); this led to a crustal configuration similar to that of the 33° 40' S transect, with a thickened crust in the current forearc (Giambiagi et al. 2015). As in the northern transect, the principal episode of shortening started in the Miocene (20–16 Ma; e.g., Silvestro et al. 2005; Sruoga et al. 2008; Mescua et al. 2014; Horton et al. 2016; Horton and Fuentes 2016; Fuentes et al. 2016).

In this segment between 35° and 36° S (Figs. 1, 3), the Andes comprise the Principal Cordillera morphotectonic province, where the Malargüe fold-and-thrust belt has been absorbing most of the shortening through the inversion of Mesozoic normal faults and newly formed Cenozoic thrusts in a “hybrid” thin- and thick-skinned deformation style (Kozłowski et al. 1993; Manceda and Figueroa 1995; Mescua et al. 2014; Fuentes et al. 2016). From the Miocene to the present day, the shortening estimates are approximately 25 km for the eastern flanks of the Principal Cordillera and 15–20 km for the western Principal Cordillera, amounting to a total of 40–45 km of shortening (Mescua et al. 2014). The calculated shortening rates are lower than in the northern transect and amount to values between 0.75 mm/year during the Early Miocene and 1.5 mm/year in the Middle Miocene (Mescua et al. 2014).

South of 35° S, an eastward arc expansion occurred during the Middle to Late Miocene (Ramos and Folguera 2011); in the Pliocene–Quaternary, the magmatic arc was established in the Principal Cordillera, to the east or on top of the vestiges of the Miocene arc (Kay et al. 2006).

## Crustal composition and direction of tectonic transport

It has been proposed that the lower crust underneath the northern (33° 40'–35° S) and southern segments (35°–36° S) is characterized by different thicknesses and compositions (Tassara and Yáñez 2003; Tassara et al. 2006; Giambiagi et al. 2012; Marot et al. 2014). The entire region was part of the Permian–Triassic Choiyoi Silicic Large Igneous Province (Llambías et al. 1993; Sato et al. 2015; Kimbrough et al. 2015), resulting in a felsic upper-crustal composition in the whole study area (Furlani 2012; Bastías-Mercado et al. 2020). Subsequently, the region encompassing both transects underwent a different tectonic evolution. While to the north of 35° S, the Mesozoic extension that caused subsidence in the Neuquén Basin was localized in a narrow, NNW-oriented zone, south of 35° S rifting was more pronounced, leading to substantial crustal thinning (Vergani et al. 1995; Giambiagi et al. 2012; Sigismondi 2012). In addition to variable crustal thickness, compositional changes along strike have been

proposed. For example, compositional differences between the two transects have been inferred from gravity modeling (Tassara et al. 2006; Tassara and Echaurren 2012; Rodríguez Piceda et al. 2020). These studies suggest a decrease in the depth of the density discontinuity between upper and lower crust toward the south (Fig. 2a), which would be linked to a more mafic composition south of 35° S. As mentioned earlier, Tassara and Yáñez (2003) estimated the elastic thickness ( $T_e$ ) to be lower than 10 km for the segment to the north of 34° S and above 20 km south of 35° S (Fig. 2a); they proposed that this difference can be explained by a change to more mafic crustal compositions south of 34° S. Marot et al. (2014) imaged the seismic structure from 29° S to 35° S and interpreted that reduced seismic velocities in the Andean lower crust can be explained by felsic compositions, either related to the accreted Chilena suspect terrane or a mafic, non-eclogitized crust (Marot et al. 2014).

Based on gravity modeling, Rodríguez Piceda et al. (2020) suggest that low densities characterize the crust below the orogen north of 35° S; while south of this latitude, the crust has a higher density (Fig. 2b). To the east, in the Andean foreland, low to intermediate densities have been calculated between 34° 30' S and 37° S, and thinner and denser crust has been inferred for the region between 37° and 39° S (Rodríguez Piceda et al. 2020). In contrast to the region of the northern transect, these variations of crustal composition likely influenced Andean mountain building by strengthening the crust south of 35° S due to its more mafic, and hence greater mechanical strength (Kusznir and Park 1986; Giambiagi et al. 2012).

An ongoing debate in Andean tectonics concerns the direction of tectonic transport along the main detachments that accommodate upper-crustal horizontal shortening. At crustal scale, a major detachment underlying the orogen is located between a 10- and 12-km depth according to cross-section balancing and geophysical modeling (Manceda and Figueroa 1995; Farías et al. 2010; Tassara and Echaurren 2012; Turienzo et al. 2012; Giambiagi et al. 2003a, 2012, 2015; Mescua et al. 2014). In light of this, an eastward-directed tectonic transport has been proposed, whereby the different morphotectonic units have been successively uplifted along these west-dipping detachment levels (Fig. 3) from west to east (e.g., Ramos et al. 2004; Farías et al. 2010; Astini et al. 2010; Giambiagi et al. 2012; Turienzo et al. 2012; Buelow et al. 2018). Cegarra and Ramos (1996) estimated shortening in the area of the Aconcagua fold-and-thrust belt (32° 50' S) to be on the order of ~60 km, while other studies estimated approximately 70 km of total shortening (Giambiagi and Ramos 2002; Farías et al. 2010; Giambiagi et al. 2012, 2015).

Conversely, Armijo et al. (2010) and Riesner et al. (2018) suggested that the region of the southern Central Andes between 33° and 34° S is underlain by the West Andean Thrust

(WAT), a principal east-dipping detachment, which accommodates westward-directed tectonic transport that has been associated with a migration of deformation from the Cordillera Frontal to the west. In this model, the WAT roots in the lower crust beneath the Frontal Cordillera and gently rises toward the western flank of the Andes, where it emerges in the Central Depression, in a thrust known as the San Ramón Fault (Armijo et al. 2010). These authors proposed that the deformation in this sector of the Andes started at ~20–25 Ma within the Frontal Cordillera and subsequently propagated westward, with the Aconcagua fold-and-thrust belt being coevally and passively transported as a secondary back-thrust structure. This model predicts low amounts of shortening between ~8 and 12 km (Riesner et al. 2018) for the Aconcagua fold-and-thrust belt, while the amount of total orogenic shortening has been estimated to range between 31 and 55 km.

More recently, Lossada et al. (2020) using thermochronologic, structural, and stratigraphic data concluded that the uplift of the Frontal Cordillera began between 15.3 and 17 Ma. In light of these new data, the eastward advance of Neogene shortening, beginning within the Aconcagua fold-and-thrust belt at ~20 Ma in the west (Ramos et al. 1996) and reaching the Frontal Cordillera and adjacent areas to the east between 17 and 15.3 Ma (Buelow et al. 2018; Lossada et al. 2020), appears to be a realistic scenario in light of previous field-based studies. We will contribute to the debate of these controversial issues by modeling horizontal shortening at lithospheric scale and discussing some of the factors that can control the direction of tectonic transport.

## Geodynamic modeling method

### Governing equations

In our modeling efforts, we used ASPECT (Advanced Solver for Problems in Earth's ConvecTion; Kronbichler et al. 2012; Heister et al. 2017; Bangerth et al. 2018), a highly scalable, geodynamic open-source code, to develop the 2D numerical models used to study deformation structures of the southern Central Andes. The incompressible material deformation is governed by solving the coupled system of momentum (Eq. 1), mass (Eq. 2), and energy (Eq. 3) conservation equations below:

$$-\frac{\partial P}{\partial x_i} + \frac{\partial \tau_{ij}}{\partial x_j} + \rho g_i = 0, i, j = 1, 2, \quad (1)$$

$$\frac{\partial v_i}{\partial x_i} = 0, \quad (2)$$

$$\rho C_p \frac{dT}{dt} = \frac{\partial}{\partial x_i} \left[ \lambda(x_i, T) \frac{\partial T}{\partial x_i} \right] + H, \quad (3)$$

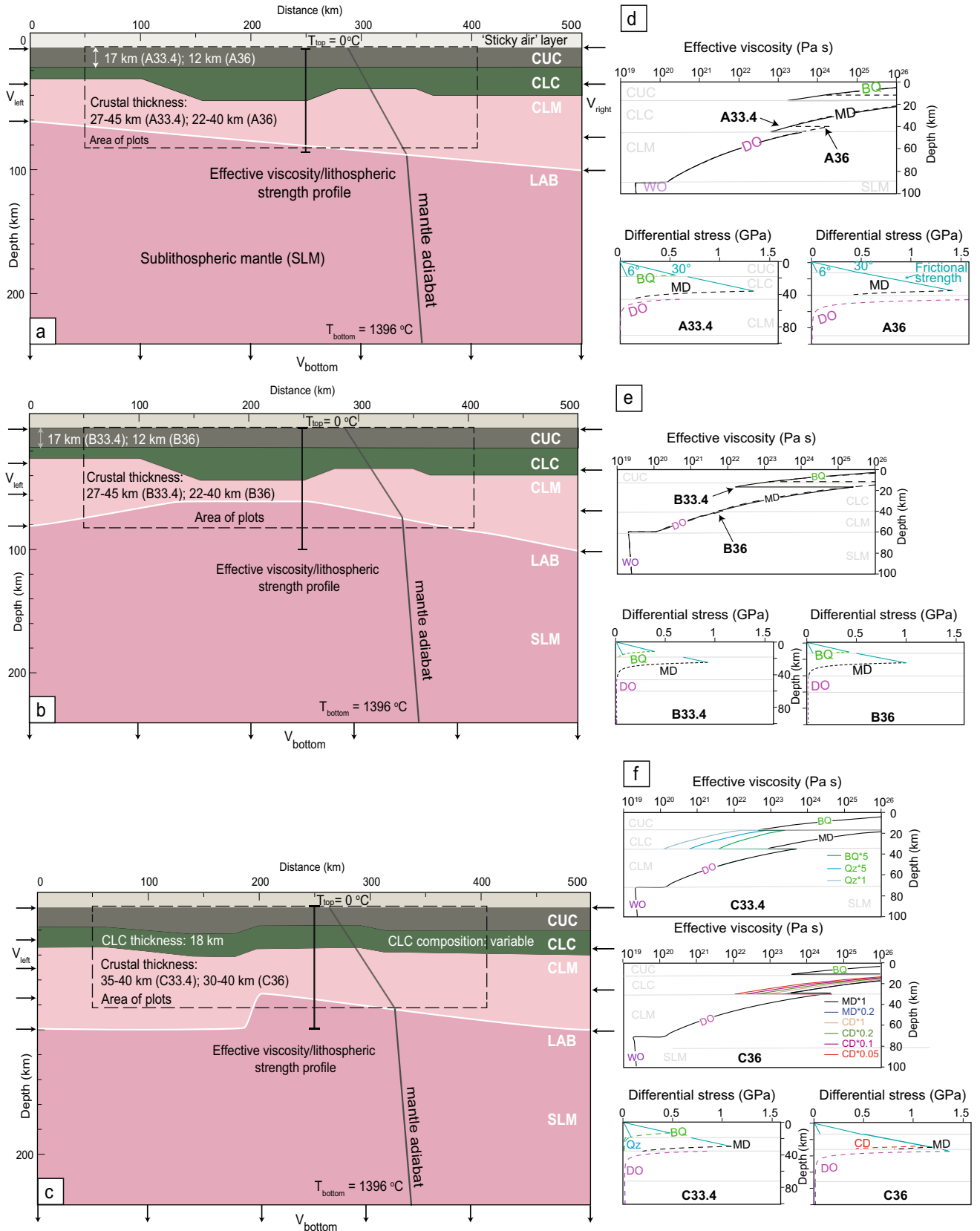




**Fig. 4** Initial numerical model setups. **a–c** A-, B-, and C-group, respectively. Material inflows ( $V_{\text{left}}$  and  $V_{\text{right}}$ ) on both lateral boundaries are balanced by a uniform outflow ( $V_{\text{bottom}}$ ) at the bottom boundary of the model. **d–f** Diagrams showing an example of the initial effective viscosity and lithospheric strength profiles from the surface to 100-km depth, calculated using the initial thermal structure (olive green line in Fig. 4a–c) and a strain rate of  $10^{-15} \text{ s}^{-1}$ . Note that strain rate varies during model evolution. Material parameters are given in Table 1. BQ=Black Hills quartzite (Gleason and Tullis, 1995); Qz=quartzite (Ranalli and Murphy 1987); MD=Maryland diabase and CD=Columbia diabase (Mackwell et al. 1998); DO=dry olivine and WO=wet olivine with constant water content (Hirth and Kohlstedt 2003). When a scaling factor is applied to the viscosity of the material, it is labeled as “\*0.1” after the name of the material (e.g., MD\*0.2). Blue lines show frictional strength for unsoftened ( $\varphi=30^\circ$ ) and softened ( $\varphi=6^\circ$ ) material in the upper crust

where the Einstein notation applies, and  $x_i$  are coordinates,  $v_i$  is the velocity,  $P$  is pressure,  $\tau_{ij}$  is the deviatoric stress tensor,  $d/dt$  is the time derivative,  $\rho$  is the density,  $g_i$  is the gravitational acceleration vector,  $T$  is the temperature,  $C_p$  is the heat capacity,  $\lambda$  is the thermal conductivity, and  $H$  is volumetric heat source including radiogenic heat, shear heating, and adiabatic heating.

## Model geometry

To investigate the crustal deformation in the two transects, we simulated the process of intraplate lithospheric shortening without taking into account the entire subduction system, as the subduction parameters between  $33^\circ$  and  $36^\circ$  S are similar. The 2D model domain is 500-km wide and 240-km deep (Fig. 4), with a variable resolution. The resolution is 500 m per element in the upper part of the lithosphere at 0–50-km depth, 1 km at 50–100-km depth, and 5 km at 100–240-km depth. This high resolution ensures that the crustal shear zones are well resolved.

We compute two main model sets, one for the northern transect at  $33^\circ 40'$  S (M33.4 models) and the other for the southern transect at  $36^\circ$  S (M36 models). The main differences between both sets are: (i) the estimated amount of applied shortening (70 km for M33.4 and 45 km for M36); (ii) the initial crustal thickness across the orogen; and (iii) the crustal composition, based on geological and geophysical constraints.

For the crustal structure, we considered a thicker crust (~40 km) in the western zone, where the Coastal Cordillera is located. This represents the Late Cretaceous shortening episode, accounting for 10 km of shortening in the M33.4 transect (Giambiagi et al. 2015). The M36 transect is not well constrained, but presumably the onset of shortening in the Late Cretaceous led to a similar configuration as in the M33.4 transect with a thickened crust in the current forearc area.

## Material properties and boundary conditions

All materials have a visco-plastic rheology. At deviatoric stress below frictional-plastic yield stress ( $\tau_Y$ ), materials deform viscously with an effective viscosity ( $\eta_{\text{eff}}$ ) given by:

$$\eta_{\text{eff}} = f \frac{1}{2B^{1/n}} \dot{\epsilon}_{\text{II}}^{\frac{(1-n)}{n}} \exp\left(\frac{E + PV}{nRT}\right), \quad (4)$$

where  $f$  is a scaling factor;  $\dot{\epsilon}_{\text{II}}^2 = \frac{1}{2} \dot{\epsilon}_{ij} \dot{\epsilon}_{ij}$  is the second invariant of the deviatoric strain rate;  $\dot{\epsilon}_{ij} = \frac{1}{2} \left( \frac{\partial v_i}{\partial x_j} + \frac{\partial v_j}{\partial x_i} \right)$ ;  $R$  is the gas constant;  $B$ ,  $n$ ,  $E$ , and  $V$  are the laboratory viscosity parameters. The scaling factor ( $f$ ) was used for linearly scaling the effective viscosity upward or downward to approximate strength variations associated with uncertainties in the laboratory-derived parameters (Beaumont et al. 2006).

The frictional-plastic deformation is responsible for faulting and follows a pressure-dependent Drucker–Prager yield criterion:

$$\tau_Y = P \sin \varphi + C_0 \cos \varphi, \quad (5)$$

where  $P$  is pressure,  $\varphi$  is the angle of internal friction and  $C_0$  is the cohesion. Materials in the upper crust undergo frictional-plastic strain softening through a decrease in the friction coefficient ( $\mu = \tan \varphi$ ) from 0.5 to 0.1 (corresponding to a change of  $\varphi$  from  $30^\circ$  to  $6^\circ$ ) and  $C_0$  from 20 to 4 MPa over accumulated strain of 0.5–1.5 (Table 1), as an approximation of material softening that agrees with previous estimates (e.g., Babeyko and Sobolev 2005; Liu and Currie 2016; Liu 2020).

The rheological parameters for the different materials are taken from laboratory experiments (Table 1): for the felsic upper continental crust (CUC), we used the properties of the Black Hills quartzite, with no melt (BQ; Gleason and Tullis 1995); for the mafic lower continental crust (CLC), we used the Maryland diabase (MD) or Columbia diabase (CD; Mackwell et al. 1998) and the felsic components correspond to the Black Hills quartzite (BQ; Gleason and Tullis 1995) or quartzite (Qz; Ranalli and Murphy 1987); the continental lithospheric mantle (CLM) is represented by dry olivine (DO; Hirth and Kohlstedt 2003); and the sublithospheric mantle (SLM) corresponds to wet olivine with constant water content (WO; Hirth and Kohlstedt 2003).

The boundary condition at the top of the experiments is zero traction, with a 10-km-thick sticky air layer (Fig. 4). This layer was used to approximate the free surface in a way that diminishes the grid distortion and the associated numerical instabilities (e.g., Schmeling et al. 2008). We applied a constant horizontal shortening rate of 1 cm/year, which is an average estimate for the southern Central Andes for the late Cenozoic (Oncken et al. 2006). Velocities are only imposed on the lithosphere at each of the lateral margins to drive lithospheric shortening.

**Table 1** Material parameters used in the models

Material properties Flow law	Black Hills quartz- ite (BQ)	Quartzite (Qz)	Maryland diabase (MD)	Columbia diabase (CD)	Dry olivine (DO)	Wet olivine (WO)
Phase	Upper crust/lower crust	Upper crust/lower crust	Lower crust	Lower crust	Lith. mantle	Sublith. mantle
Density, $\rho_0$ (kg/m <sup>3</sup> )	2800	2800	3000	3000	3250	3300
Heat expansion, $\alpha$ (K <sup>-1</sup> )	3.70E-05	3.70E-05	2.70E-05	2.70E-05	3.00E-05	3.00E-05
Specific heat, $C_p$ (kJ kg <sup>-1</sup> K <sup>-1</sup> )	1.2	1.2	1.2	1.2	1.2	1.2
Thermal con- ductivity, $k$ (W K <sup>-1</sup> m <sup>-1</sup> )	2.5	2.5	2.5	2.5	3.3	3.3
Thermal productiv- ity, $A$ ( $\mu$ W m <sup>-3</sup> )	1	1	0.3	0.3	0	0
Friction angle, $\varphi$ (°)	30–6	30–6	30	30	30	30
Cohesion, $C_0$ (MPa)	20–4	20–4	40	40	40	40
Dislocation creep pre-exponential factor, $B$ (Pa <sup>-n</sup> s <sup>-1</sup> )	8.57E-28	8.12E-20	5.78E-27	1.37E-25	6.22E-16	2.03E-15
Dislocation creep activation energy, $E$ (kJ mol <sup>-1</sup> )	223	156	485	485	480	480
Dislocation creep activation volume $V$ (cm <sup>3</sup> mol <sup>-1</sup> )	0	0	0.3	0	11	11
Power law expo- nent, $n$	4	2.4	4.7	4.7	3.5	3.5

Below the lithosphere, the condition of the boundaries at the lateral margins is no slip. We added a small outflux velocity ( $V_{\text{bottom}}$  in Fig. 4) to the bottom boundary to maintain the mass balance. In addition, we tested different boundary conditions by prescribing the velocity of either 0.5 cm/year on both lateral boundaries or 1 cm/year on one side of the boundary and 0 cm/year on the other side, respectively. The differences in the model behavior with these velocity conditions are minor and, thus, negligible. The resulting total shortening is 70 km for the M33.4 and 45 km for the M36. Given the estimates of very low erosion rates that have prevailed at this latitude since the Miocene (Val et al. 2018; Stalder et al. 2020), no erosion was applied to the models.

The temperature settings were set to 0 °C at the surface and 1396 °C at the bottom of the model. The initial temperature distribution is linear from the bottom of the lithosphere to the surface and adiabatic between the lithosphere–asthenosphere (LAB) boundary and the bottom of the model. The lateral boundaries of the asthenosphere have conductive geotherms and no horizontal heat flux.

### A-group models: linear LAB

The first model setup (A-group models; Fig. 4a) consists of two models for each cross section, at 33° 40' S (A33.4) and at 36° S (A36), respectively. For the A33.4 models, the crust has a 17-km-thick upper crust and a maximum thickness of 45 km; while in the A36 models, the upper crust is 12-km thick and the maximum crustal thickness is 40 km. In an attempt to simulate the initial crustal configuration, both setups have an irregular Moho geometry before the Miocene shortening phase when the crust was already thickened in the westernmost zone (cf. Sect. 2). For both models, the depth of the LAB linearly increases from 60 km on the left (western) side of the model to 100 km on the right (eastern) side, on the assumption that the lithosphere is thicker in the Andean foreland (Tassara and Echaurren 2012).

### B-group models: symmetric LAB

In this model setup, the crustal structure is the same as in the previous model group (A-group). The main difference

in this group (B33.4 and B36 for each transect) is the geometry of the LAB (Fig. 4b), which is modified to replicate the geometry influenced by the mantle-wedge corner flow, with a thinner lithosphere where the corner flow develops (e.g., similar to the LAB in Fig. 3). This configuration relies on the assumption that subduction processes were already ongoing since the Late Permian (Oliveros et al. 2018). This approach simulates the temperature distribution and strength characteristics of the lithosphere according to its thickness. In these models, the materials and rheology used are the same as in the A-group models.

### C-group models: asymmetric LAB

In the C-group models (Fig. 4c), the geometry of the LAB was changed to better simulate the structure of the lithosphere near the subduction zone. An asymmetric simplified LAB geometry was used to replicate the lithospheric strength and heat distribution in the orogen and to test its effect on deformation (Fig. 4c). This simplified geometry follows the LAB modeled by Tassara and Echaurren (2012), as shown in Fig. 3, with a thicker lithosphere at the western side of the model (i.e., present-day forearc) and the thinnest part located at  $x$ -coordinates 200 km (beneath the present-day orogen); the thickness was subsequently and progressively increased toward the east. We also changed the crustal geometry based on the structural reconstructions by Giambiagi et al. (2015) for the Late Cretaceous (cf. Section 2). A minimum crustal thickness of 30 km was assigned to the C36 models, where a more generalized extension than that of the C33.4 models occurred ( $x$ -coordinates: 200–290 km; Fig. 4c). A thicker crust (35 km) was assigned to C33.4 (cf. Sect. 2).

Another variation that we introduced here relates to the composition of the lower crust, and hence its rheology. To investigate the effect of this factor, we set the thickness of the lower crust to 18 km by varying the thickness of the upper crust (Fig. 4c, f). As mentioned in Sect. 2, the crust was likely modified during the pre-Andean tectonic evolution (e.g., Kleiman and Japas 2009; Sigismondi 2012; Giambiagi et al. 2012). For the models representing the 33° 40' S transect (C33.4), a more felsic lower crust was used; while in the southern zone, a mafic lower crust was selected. For the C33.4 model (C33.4), we considered a quartzite (Qz) and a Black Hills quartzite (BQ) to represent the material parameters of the lower crust. We also applied a scaling factor  $f=5$  to the dislocation creep flow of these materials (e.g., Currie and Beaumont 2011; Liu and Currie 2016; Wolf and Huisman 2019) to account for uncertainties related from extrapolating from laboratory experiments to nature. This implies a stronger rheology than a quartzite material and helps to simulate a more intermediate composition for the lower crust.

For the model run representing the transect at 36° S (C36), we used either the Maryland diabase (MD) or the Columbia diabase (CD) for the mafic lower crust, the latter being weaker than the former (Fig. 4f, Burov 2011). In addition, we applied scaling factors  $f$  of 0.2 and 1 for the Maryland diabase, and 0.05, 0.1, 0.2, and 1 for the Columbia diabase, to simulate the strength of a lower crust that has been affected by temperature and melting in the area corresponding to the volcanic arc.

## Results

We ran more than 60 models grouped into the three previously described setups. We present the results below and summarize them in Table 2. Taken together, our modeling results clearly show that the lower-crustal composition is an important factor that controls the mode of deformation and that the asymmetric geometry of the lithosphere–asthenosphere boundary (LAB) apparently triggers eastward-directed crustal deformation.

### A-group models (linear LAB)

Figure 5 shows the second invariant of the strain rate for the A-group models. From this group of models, we observe that deformation occurs where the lithosphere is thinner (near the left boundary), although the crust is also thinner in the same zone. The crustal thinning increases the integrated strength of the lithosphere when compared to a lithosphere with a thicker crust (Fig. 4d). We note, however, that the western (left) boundary of the model box combined with the thinnest lithosphere may also concentrate deformation.

In the A33.4 model, the deformation is focused on the left side of the model box (forearc) and, despite some deformation observed to the east ( $x$ -coordinates: 120–150 km), is considered minor; instead, the underthrusting of the crust at the western border of the model occurred after ~ 50 km of shortening (Fig. 5a–c).

For the A36 model, the results are similar to that of the A33.4 model: Deformation almost exclusively affects the left side of the model, with underthrusting of the eastern crust to the west (Fig. 5d–f) after 45 km of shortening. In these cases, the deformation is mostly concentrated associated with a principal thrust fault that cuts the entire crust (e.g., Fig. 5f M#10); in the equivalent model A33.40 (Fig. 5a M#6), however, the deformation is more complex and results in a pair of main detachments. We interpret this to be the result of a thicker mafic crust in the A36 models, which provides greater strength for the whole crust. In general, all of these models deform with east-directed (i.e., west-dipping), first-order structures associated with thrusting.

**Table 2** Main characteristics of each group of models

M#	Model group	CUC thickness (km)	Max. crustal thickness (km)	LAB geometry	CLC composition
6	A33.4	17	45	Linear	MD
10	A36	12	40		MD
12	B33.4	17	45	Symmetric	MD
14	B36	12	40		MD
16	C33.4	Variable	40	Asymmetric	MD
22	C33.4	Variable	40		Qz
23	C33.4	Variable	40		Qz*5
24	C33.4	Variable	40		BQ*5
18	C36	Variable	40		MD
34	C36	Variable	40		CD*0.2
35	C36	Variable	40		CD
36	C36	Variable	40		MD*0.2
39	C36	Variable	40		CD*0.1
40	C36	Variable	40		CD*0.05

Note that number of models (M#) are non-correlative. CUC: continental upper crust. CLC (continental lower crust) composition: MD and MD\*0.2: Maryland diabase with the value of the scaling factor  $f=1$  or 0.2; Qz: Quartzite scaling factor 1; Qz\*5: Quartzite with  $f=5$ ; BQ\*5: Black Hills quartzite with  $f=5$ . CD0.2, CD, CD\*0.1, CD\*0.05: Columbia diabase with  $f=$  from 0.05 to 1

However, the A-group models do not replicate the deformation patterns determined from geological and geophysical data in the Andes. One main conclusion from this set of experiments is that deformation is focused where the lithosphere is thinner and, thus, weaker (e.g., Kusznrir and Park 1986), in this case close to the left side of the model box.

### B-group models (symmetric LAB)

In these models, the lithospheric thickness varies symmetrically along the geological cross section (Fig. 4b). Deformation is mostly focused where the lithosphere is thinner, between  $x$ -coordinates 150 and 300 km (Fig. 6). This would closely replicate the deformation in the arc region of the orogen, where due to corner flow, the lithosphere is thinner and, thus, susceptible to deformation under compression. At the beginning of the model run (~5-km shortening, Fig. 6a, d), deformation is visible in the upper crust as a pair of conjugate faults or shear zones that radiate from a point at the boundary between the upper and lower crust; subsequently, these faults propagate downward to the LAB, in very diffuse zones (Fig. 6b, e). In the B33.4 models, after 40 km of shortening, the deformation is concentrated along a main thrust fault, which either dips westward (M#11 with velocity applied on both sides of the model; not shown here) or eastward (M#12; Fig. 6b). We ran these models a second time with the same setup to test once more the dip of the developing detachments and found that it is randomly oriented. We interpret that this behavior is due to the homogeneity of the crust, and that once the yield strength is reached, the crust

deforms by detachments randomly dipping to the east or to the west.

Although the models reproduce a number of geological features observed in the thrust belt, they do not replicate some of the important orogenic features in the study area. For example, the crustal thickness is higher than present-day estimates. After 70 km of shortening in the M#12 model, the crust reaches a thickness of approximately 70 km; while according to Tassara and Echaurren (2012), the present-day crustal thickness is 50 km.

Similarly, in the B36 models, the dip direction of the detachments does not seem to be controlled by velocity boundary conditions. In these models, the upper crust is thinner than the B33.4 models and the deformation pattern is different (Fig. 6d–f). We observe that the location of the crustal shear zone (labeled as “main thrust fault” in Fig. 6f) is controlled by the change from thinner to thicker crust established during the initial conditions for model B36.

### C-group models (asymmetric LAB)

Here, we present the most relevant results from a total of 20 C-group models. In the C33.4 models, when we use a mafic material such as a Maryland diabase, the lower crust does not flow and the upper-crustal detachment roots in a lower-crustal shear zone, cutting the entire crust (Fig. 7a–c; M#16). We reproduce with these models the decoupled deformation mode, where upper- and lower-crustal deformation processes are displaced horizontally with respect to each other (Fig. 2d). This deformation mode also forms in the case of the C36 models where the Maryland or Columbia

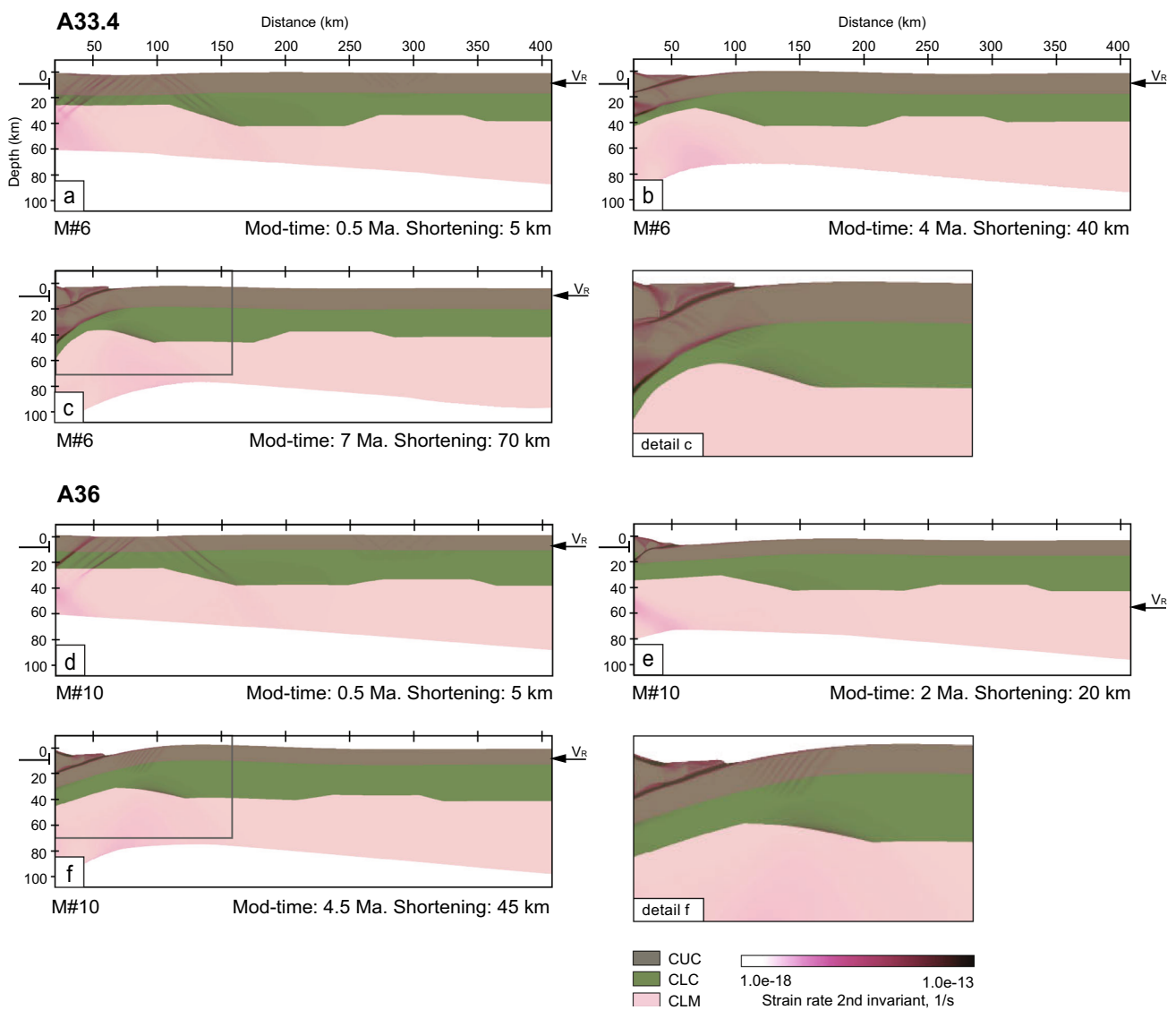


**Fig. 5** A-group modeling results. Mod-time refers to modeling time, which does not correspond to geological time. **a–c** A33.4 at different shortening stages. **a** After 5 km of shortening, shear zones have developed in the upper crust. **b** Shortening is accommodated along a main shear (thrust fault) zone. **c** After 70 km of shortening; deforma-

tion affects only the thinner part of the lithosphere on the left side of the model with accompanying underthrusting of the crust. **d–f** A36 at different shortening stages. As in the A33.4 models, deformation is always focused in the thinner part of the lithosphere on the left side of the model

diabases are assigned to represent the mafic lower crust (Fig. 8; M#18 and M#35). Even applying a scaling factor of 0.05 to the Columbia diabase material (Table 2; M#40) to reduce the strength of the lower crust, the results are similar to a decoupled mode of deformation.

In the C33.4 models with more felsic and, thus, weaker composition of the lower crust (Fig. 7d–f; M#24), the crust flows viscously, producing a wide crustal root. This deformation is aligned vertically with upper-crustal deformation, as a pure-shear or coupled deformation mode. In addition, the crust reaches a thickness of almost 60 km after 70 km of shortening, which closely correlates with the actual crustal

thickness of the orogen, although our models do not include erosion.

All models with an asymmetric LAB (Fig. 4c) produce west-dipping thrust faults (Figs. 7, 8), which agrees with the majority of the geological models of the Central Andes. This could be interpreted as a result of the thicker and stronger lithosphere (e.g., Kusznir and Park 1986) to the left (west) of the model, which would correspond to the present-day forearc. This western domain is usually inferred to be a rigid block of cold and thick lithosphere, which acts as a backstop for the east-directed movement of the crust (Tassara and Yáñez 2003; Farías et al. 2010).

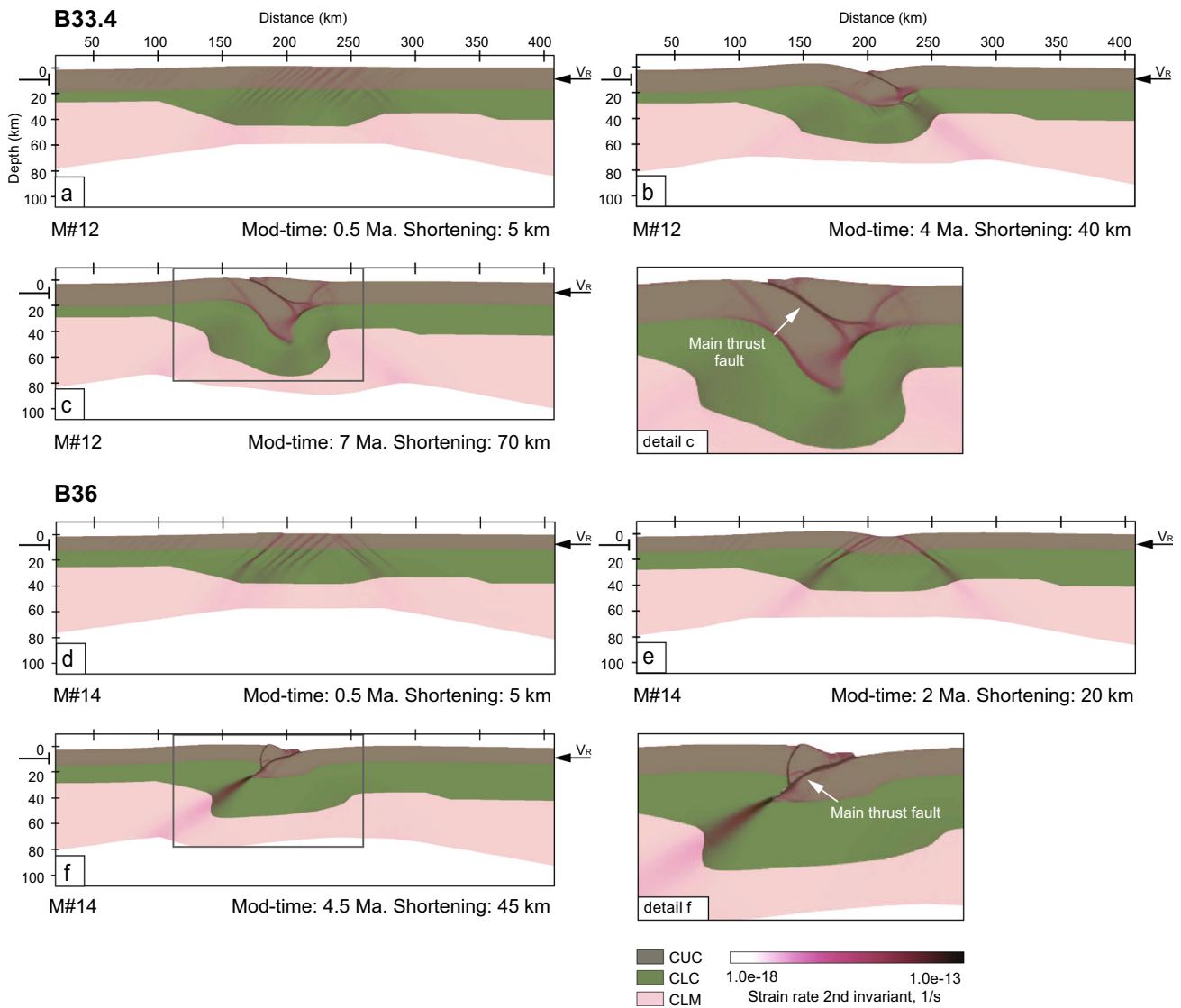


**Fig. 6** B-group modeling results. **a–c** B33.4 at different stages showing that deformation affects the thinner part of the lithosphere ( $x$ -coordinates 150–250 km). **a** Shear zones developed in the crust after 5 km of shortening. **b** With 40 km of shortening, deformation is focused along a main east-dipping thrust fault. **c** After 70 km of shortening the main thrust fault accommodates most of the defor-

mation. **d–f** B36 after 45 km of shortening. As in previous models, deformation is focused in the central part of the model box, where the lithosphere is thinner. The dip direction of the main detachments is randomly directed to the east (**f**) or the west (**c**) despite the velocity boundary condition

## Discussion

First, our modeling results show that lower-crustal composition is an important factor in controlling the mode of deformation in a mountain belt; second, the initial asymmetric geometry of the LAB is the main factor that determines the polarity of fold-and-thrust belts in a convergent, non-collisional mountain belt such as the Andes. In light of these observations and in the context of the major geological structures observed in the southern Central Andes, our modeling shows that eastward-directed crustal deformation and a foreland-directed development of structures, becoming

younger towards the east, is associated with the existence of an asymmetric LAB, which is the result of asthenospheric corner flow associated with the subduction of the Nazca plate.

## Model limitations

In our models, we tested the influence of different crustal thicknesses and compositions as well as lithospheric thickness in order to assess the lithospheric deformation style under a regime of horizontal shortening. For the models of the B- and C-groups, although the lithosphere is thinner

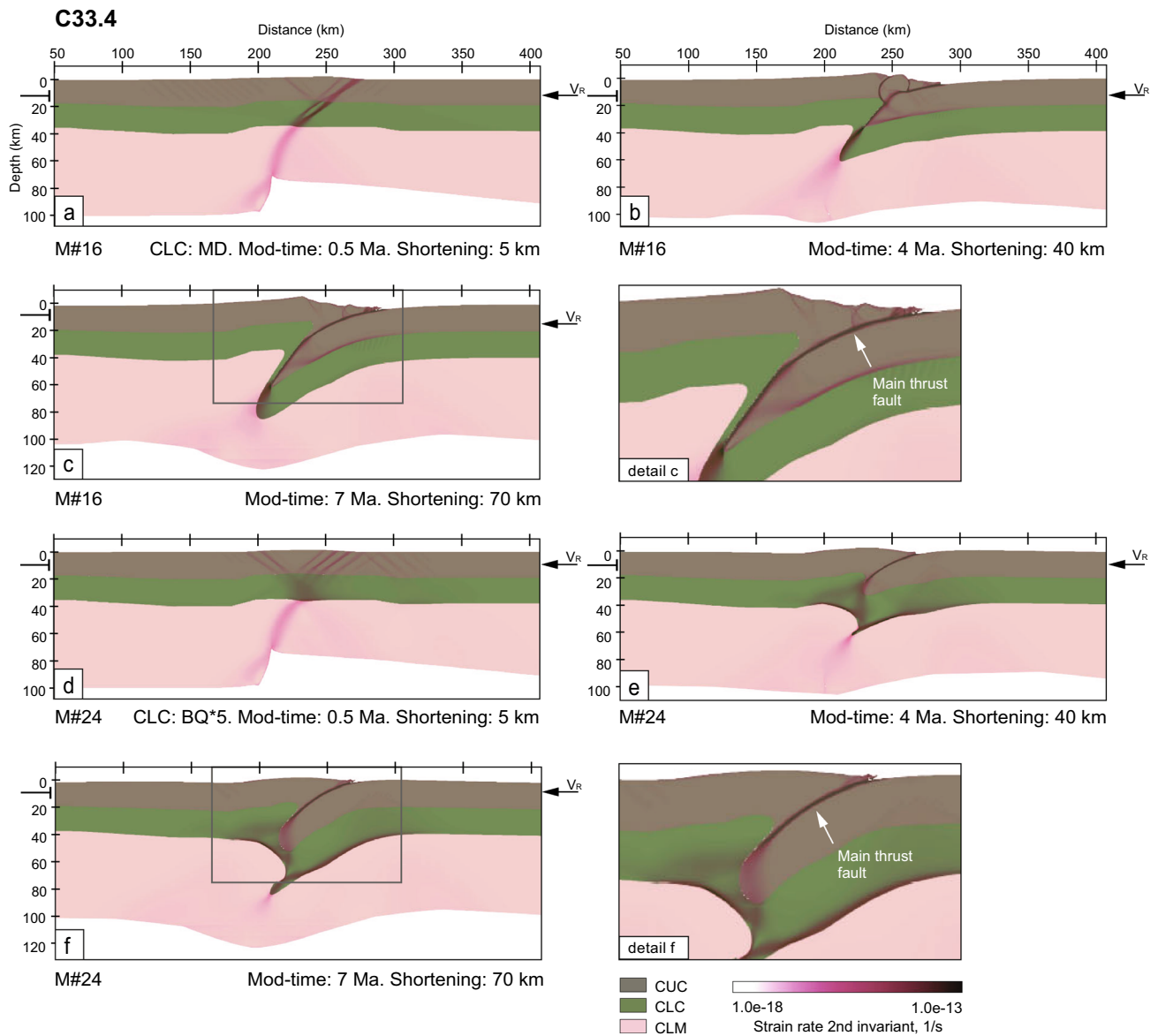


**Fig. 7** C33.4 model results with different rheological characteristics for the lower crust. Mod-time refers to modeling time. **a–c** The lower crust corresponds to a MD (Maryland diabase). **a** Initial shortening stage (5 km), where a west-dipping shear zone develops in the mantle lithosphere and in the crust. **b** After 40 km of shortening, the initial shear zone in the lithosphere leads to the development of a main west-dipping thrust that cuts the upper and lower crust. **c** At the final stage (70 km of shortening), the main thrust absorbs most of the deformation in the crust with the development of secondary

structures (backthrusts). **d–f** The lower crust corresponds to more felsic material (BQ\*5: Black Hills quartzite scaling factor 5). **d** As in M#16, the west-dipping shear zone deforms the mantle lithosphere and the crust. **e** After 40 km of shortening the main west-dipping thrust fault cuts the upper crust leading to viscous flow in the lower crust. **f** In the final stage, the thrust cuts the upper crust and roots in a diffuse zone in the lower crust where viscous flow produces thickening in the same crustal column as part of a coupled deformation mode

below the area that represents the magmatic arc, the lithospheric geometry in the model is probably still too simple as compared to the real structure. Furthermore, as our aim is to analyze these first-order variables, we do not consider either inherited crustal structures (such as faults or weak zones) or local lithological changes that could influence the local style of deformation.

The main simplification in our setup is that the simulation does not include the subduction system comprised of an oceanic plate interacting with the continental plate and underlying mantle. In particular, we focus on the deformation mode of the crust without considering the influence of the slab on the dynamics of asthenospheric corner flow. Additionally, Sobolev et al. (2006) demonstrated that

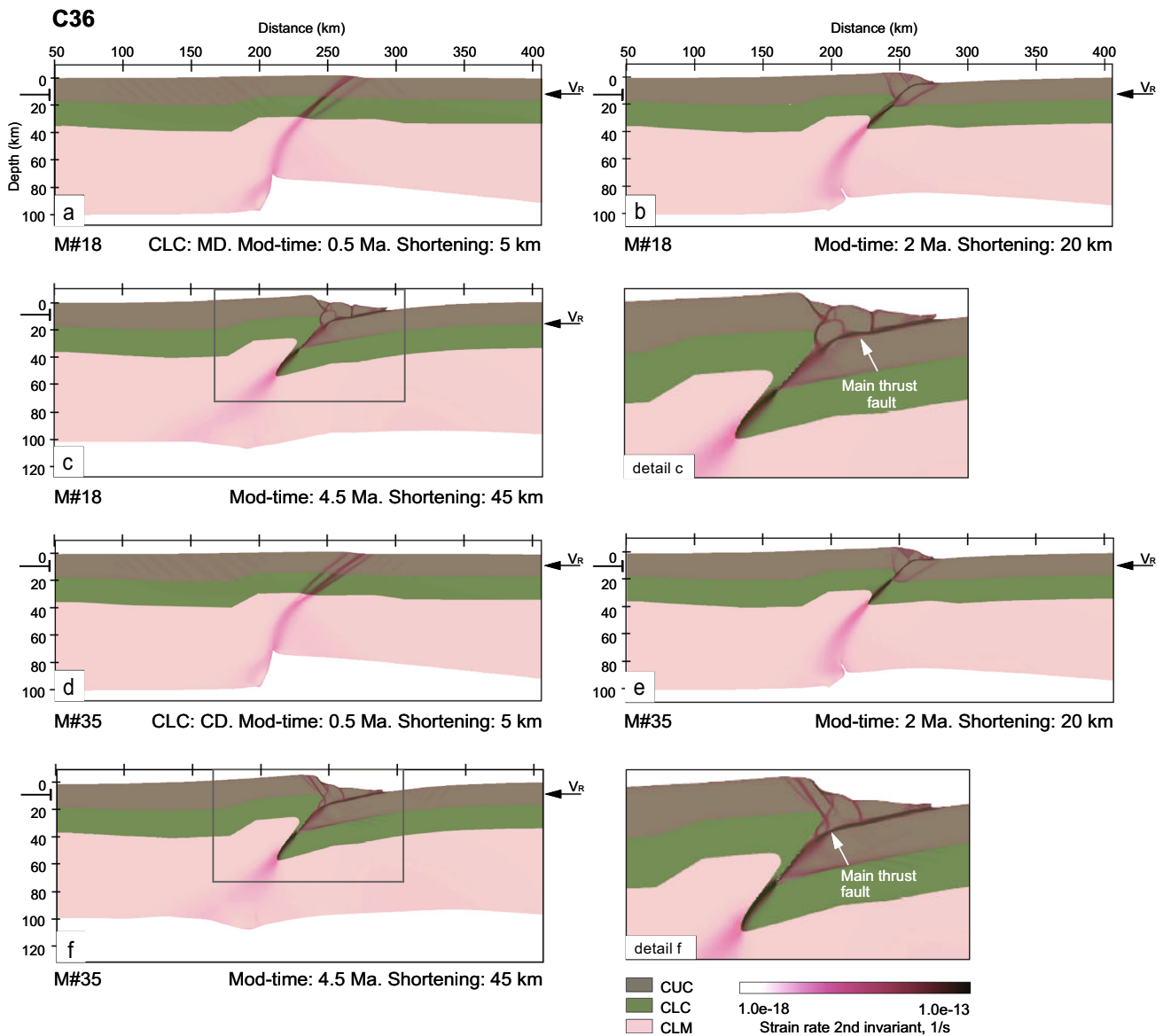


**Fig. 8** C36 model results with different, but mafic, rheologies for the lower crust. **a–c** The lower crust corresponds to a MD (Maryland diabase). **d–f** The lower crust corresponds to mafic material (CD Columbia diabase), although it is weaker than the Maryland diabase (Fig. 4f) leads to similar results as in M#18: the mafic lower crust prevents viscous flow in both cases. **a, d** As in the C33.4 models dur-

ing the initial stage, a west-dipping shear zone develops in the mantle lithosphere causing thrusting in the crust. **b, e** With 20 km of shortening the upper and lower crust are subjected to thrusting. **c, f** After 45 km of shortening, upper-crustal shortening is displaced to the right (i.e., east) with respect to lower-crustal deformation, as in the decoupled deformation mode

the main effect of asthenosphere dynamics occurs when delamination of the lithospheric mantle takes place and corner flow is blocked, producing changes in shortening rates. In our study area, there is no indication that delamination has occurred. Alternatively, the lithospheric thickening of the upper plate due to shortening could affect the corner flow, but this is beyond the scope of this paper. We plan to carry out models that include the subducting slab and mantle flow, and test their influence on the upper plate deformation in future work.

Although feedback between tectonics and surface processes exists, we did not include erosion in the models due to low-erosion rate estimates for the area (Val et al. 2018). The elapsed modeling time does not correspond to geological time; thus, the models do not start from an initial thermal steady-state condition. Here, we focused on achieving the final shortening accounted for each transect, instead of simulating the true temporal evolution.



## Role of lower-crustal composition and thickness in determining the mode of deformation

The connection between crustal composition and thickness, and the style and amount of upper-plate deformation remains poorly understood, although several studies have addressed this issue (e.g., Allmendinger and Gubbels 1996; Kley et al. 1999; Gerbault et al. 2009; Mouthereau et al. 2013; Mescua et al. 2016; Lacombe and Bellahsen 2016). Since the response of the crust to an applied stress mainly depends on the distribution of brittle and ductile strength with depth, the crustal composition is certain to be an important parameter controlling deformation (Gerbault et al. 2009; Lowry and Perez-Gussinye 2011), particularly in the lower crust (Kusznir and Park 1986). While the brittle strength is a function of pressure and depth, the ductile strength is mainly controlled by temperature, strain rate, and composition (Brace and Kohlstedt 1980; Kusznir et al. 1991; Jackson 2002; Burov and Watts 2006). According to the thermo-mechanical models carried out by Gerbault et al. (2009), the upper plate shortening is mainly controlled by upper plate rheology. In this context our models offer relevant insights into the role of the lower-crustal composition, and thus crustal strength, with respect to the overall mode of deformation. They show that a mafic and stronger lower crust results in a decoupled mode of deformation, where lower- and upper-crustal deformation are offset towards the west or east of the mountain belt, respectively (Fig. 9d–f). In contrast, a more felsic, weaker, lower crust leads to a coupled deformation mode.

To the north of the study area, in the intraorogenic Andean Plateau (Altiplano–Puna Plateau), it has been proposed that changes in the strength of the lithosphere are related to the presence of thick Paleozoic sedimentary sequences in the foreland (Allmendinger et al. 1983; Allmendinger and Gubbels 1996; Pearson et al. 2013). This scenario was tested by Babeyko and Sobolev (2005) and more recently by Liu (2020) employing numerical modeling. Their results show that the decrease of mechanical strength of the sediments in the foreland of the Altiplano sector of the plateau causes the changeover to a decoupled, simple-shear deformation mode. Interestingly, between 33 and 36° S, the thickness of the Mesozoic and Cenozoic sedimentary succession of the Neuquén Basin is similar (~4 km), suggesting that sedimentary basin thickness is not the decisive control on the mode of deformation. Instead, our models explain the change in deformation style between coupled and uncoupled modes as a consequence of variation in lower-crustal composition as a result of a different Mesozoic history. By means of gravity modeling, Ibarra et al. (2019) suggested that in the Altiplano region of the Andean Plateau, underthrusting of the more mafic foreland crust (Meeßen et al. 2018) would alter the average density of the crust in the orogen

as a whole, which is typically lower due to a more felsic composition (e.g., Götze et al. 1991; Tassara et al. 2006). Ibarra et al. (2019) proposed that the deformation focuses in the transition between the felsic, weak crust in the orogen and the more mafic, strong crust in the foreland. In our M36 models, we use layers with laterally homogeneous material properties, and we still observe the underthrusting of the more mafic lower crust due to its greater strength with respect to the upper crust.

The decoupled mode of deformation is best represented by models where the material of the lower crust is more mafic (modeled with a Maryland or Columbia diabase, M#18 and M#35, Fig. 8). Although these materials could represent an end-member condition rather strong lower-crustal characteristics, the results lead to similar when using reduced scaling factors. This is the case for the segment south of 35° S, where a mafic lower crust has been inferred based on gravity data (Tassara and Yáñez 2003). Our models show that the greater strength of such a mafic lower crust prevents its flow. Thus, deformation in the lower crust is shifted to the west compared to the deformation accommodated in the upper crust. This deformation in the lower crust is driven by a major reverse fault that cuts both lower and upper crusts.

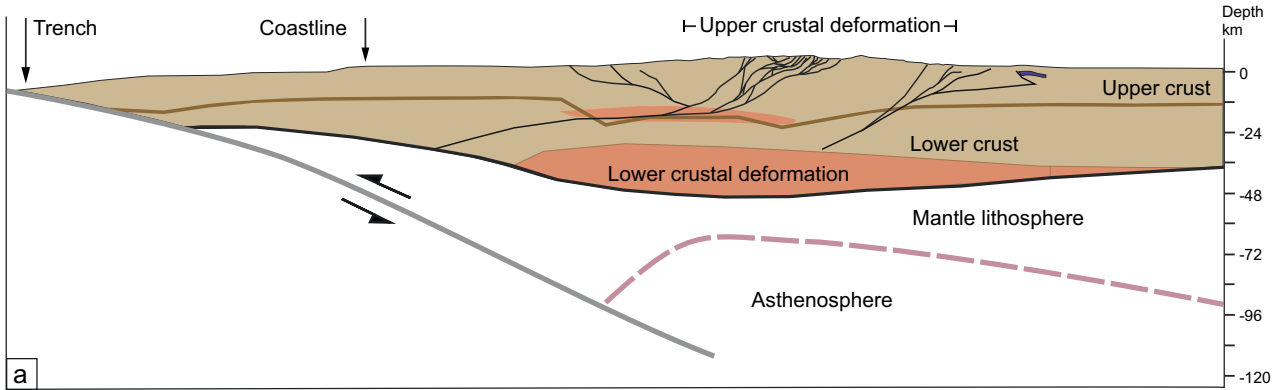
The coupled deformation mode is represented by models with a more felsic material in the lower crust (M#24, Fig. 7d–f). Considering that its composition is likely intermediate, rather than purely felsic, we apply for the lower crust a rheological model for Black Hills quartzite (BQ) with increased viscosity by a factor of  $f=5$ . In these models, the zone of thicker crust coincides with the maximum topography and upper-crustal shortening. This situation is similar to that observed for the Andes at ~33°–34°S. Our models indicate that the felsic lower crust allows viscous flow, provoking its thickening due to the compensation of shortening of the upper crust (Fig. 9b, c).

Regarding variations in the initial crustal thickness, we do not observe major changes in the mode of deformation. When comparing models with similar lower-crustal materials (i.e., Maryland diabase) and different maximum crustal thickness, the results are similar. Model results for the northern transect (e.g., M#16, Fig. 7c) with a thicker crust (max. 45 km) are akin to models for the southern transect (e.g., M#18, Fig. 8c), with a thinner crust of max. 40 km. This could be explained by the minor variations in crustal thickness values (45 km vs 40 km) tested in the models, which, however, do not contribute significantly to the strength of the crust (Fig. 4f) in a way that changes the deformation mode.

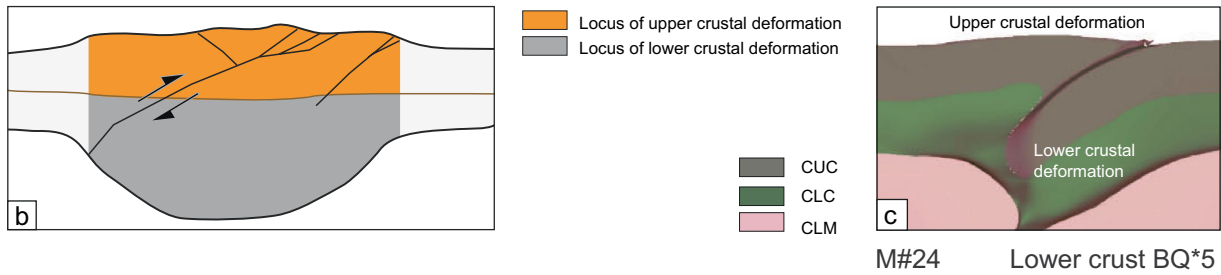
## Role of lithospheric thickness and LAB asymmetry

Subduction contributes to the asthenospheric mantle flow above the slab (e.g., Schellart 2004) and the release of

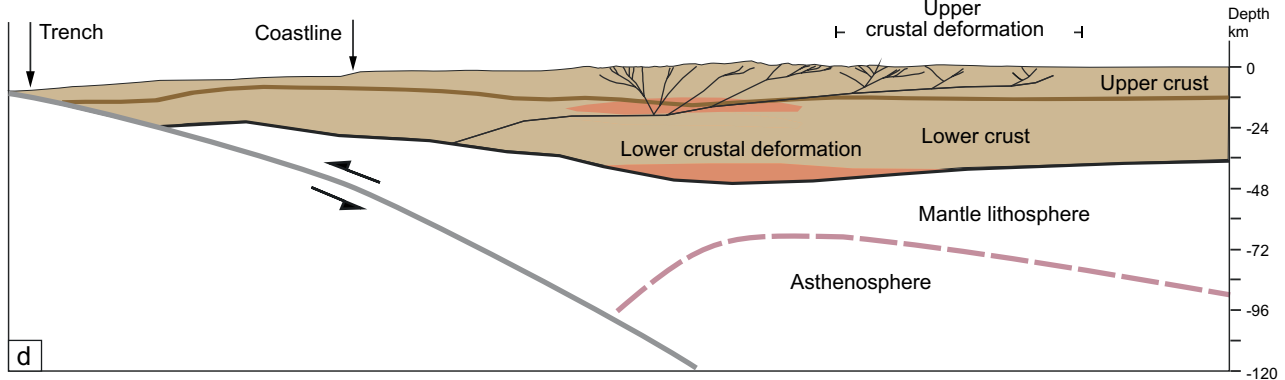
**33°40'S transect**



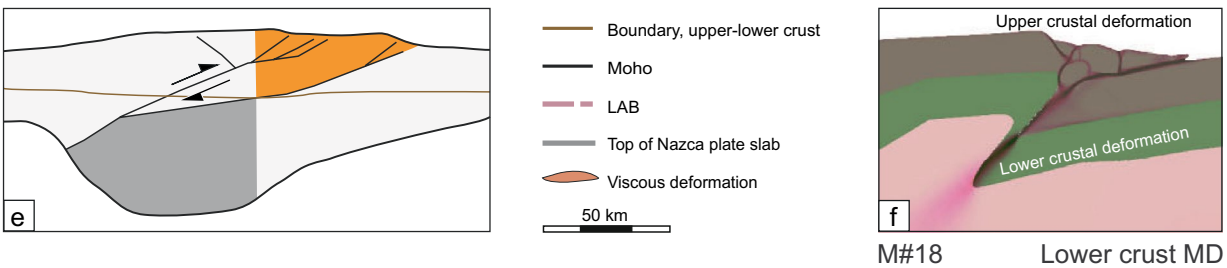
**Coupled deformation mode**



**36°S transect**



**Decoupled deformation mode**



fluids from it (e.g., Peacock 1990). Both processes weaken and thermally erode the lithospheric mantle of the upper plate (Isacks 1988; Arcay et al. 2006; Macpherson 2008; Currie et al. 2008), provoking lithospheric thinning and the development of an asymmetric lithosphere–asthenosphere

boundary (LAB). In our models, the LAB presents a marked asymmetry; it is thinner close to the subducting slab and thicker toward the foreland. This asymmetry is likely controlled by the geometry of eastward subduction and the resulting asthenospheric corner flow,

**Fig. 9** Structural transects at 33° 40' S and 36° S and preferred modeling results. **a** 33°40'S transect (modified from Giambiagi et al. 2015), where deformation in the upper crust is coupled with lower-crustal deformation (i.e., thickened crust) as shown in **b** (cartoon modified from Allmendinger and Gubbels 1996) and where the deformed upper and lower crusts are shown in orange and gray, respectively. **c** Result of the model M#24 representing the case for the 33°40'S transect with a more felsic ductile lower crust (BQ\*5: Black Hills quartzite with  $f=5$ ) that causes thickening under compression below the zone of deformation in the upper crust. **d** 36°S transect (based on Giambiagi et al. 2012; Orts et al. 2012; Astaburuaga 2014; Tapia 2015; Barrionuevo et al. 2019; Barrionuevo 2020), where the upper-crustal deformation is shifted toward the east with respect to the lower-crustal deformation as depicted in the decoupled shortening mode. **e** Upper crustal deformation shown in orange is displaced to the east with respect to the locus of lower-crustal deformation depicted in gray (cartoon modified from Allmendinger and Gubbels 1996). **f** Result of the model run M#18 representing the southern transect, where a mafic (MD Maryland diabase) lower crust provokes a shift in the loci of upper- and lower-crustal deformation

which provokes an asymmetrical thermal thinning of the lithosphere.

Regarding the lithospheric thickness, our results indicate that, for all the tested geometries of the LAB, deformation is concentrated where the lithosphere is thinner, in accordance with the thermo-mechanical models from Gerbault et al. (2009). In the A-group models, the deformation focuses on the left side of the model box where the lithosphere is thinner, and thus weaker, although the crust is thinner (stronger) in the same area. For the B- and C-groups, the lithosphere is thinner in the central part of the model box, and it is, thus, more prone to deform at this location.

The classic paradigm for the southern Central Andes states that the tectonic transport of crustal material occurs in an east-directed manner, with sequential stacking of thrust sheets from the arc to the foreland region (Ramos et al. 2004; Farias et al. 2010; Giambiagi et al. 2015; Horton 2018). This paradigm, however, has been recently challenged by a west-directed model proposed by Armijo et al. (2010) and Riesner et al. (2018). This model proposes the underthrusting of the rigid block of the forearc beneath the Andean orogenic system, whereby deformation is driven by the east-dipping West Andean thrust, which cuts the entire crust and the Moho. As such, this configuration resembles pro-shear zones, which have been modeled in continent–continent collision zones (Willett 1999; Beaumont et al. 1996) with an overall symmetric LAB and thickening below the orogenic axis.

Based on our results, we propose that the tectonic transport of the orogenic system is primarily controlled by the asymmetry of the LAB. In models with a symmetric LAB, the dip of the main detachments is randomly oriented without a control by velocity boundary conditions.

The geometry of the models with an asymmetric LAB (C-group) delineates a thick and strong lithosphere in the

western part of the model, which represents the forearc acting as backstop or a rigid indenter as proposed for the Andean plateau (Tassara and Yáñez 2003). This rigid block induces deformation that is directed to the east, in accordance with the regional geological observations (Coutand et al. 2001; Elger et al. 2005; Scheuber et al. 2006). Farias et al. (2010) proposed a similar model of the forearc as a rigid indenter with east-directed deformation for our study area.

An interesting topic to assess is the influence of climate-driven erosion and its effects on orogenic structure and faulting, as it has been shown that a feedback mechanism may exist between these two processes (e.g., Davis et al. 1983; Willet 1999). As proposed by Willett (1999), the topographic profile of an orogen, in the absence of erosion, is asymmetric with the steeper slope on the retro-wedge side; the exhumation pattern is asymmetric as well in that case, being higher in the retro-wedge. Under asymmetric erosional conditions focused on the retro-wedge area, exhumation is increasingly localized toward the foreland. If erosion is higher in the pro-wedge (i.e., toward the subducting plate) the exhumation pattern widens to the orogen interior. Although there is a precipitation gradient across the Andes in our study area (Hoke et al. 2013), this region has remained in a long-lasting semi-arid corridor (Hinojosa and Villagran 1997). Interestingly, between 28° and 36° long-term erosion rates have remained low on both sides of the orogen (Val et al. 2018) unlike areas to the north (e.g., Strecker et al. 2007; Bookhagen and Strecker 2012) and the south (e.g., Thomson et al. 2010; Georgieva et al. 2019). Thus, the climatic conditions in the semi-arid orogenic wedge of the southern Central Andes appear to have never been able to influence the direction of tectonic transport, although when viewed at finer spatial scales, the level of activity of individual thrust sheets in the orogenic wedge of the investigated area may have been influenced by a combination of tectonic processes and superposed climate-driven surface processes (Hilley et al. 2004). We, therefore, conclude that the overall tectonic character in this part of the mountain range is mainly a function of the geometry of the lithosphere–asthenosphere boundary and inherited heterogeneities.

Of all the tested models, the results of the C-group best reproduce the observed deformation for this sector of the Andes. Models M#24 (Fig. 9c) and M#23 are consistent with the geological and geophysical inferences for the 33°40'S transect, while models M#18 (Fig. 9f) and M#35 are compatible with the structural characteristics of the 36°S transect. The conceptual model postulated by Giambiagi et al. (2012) is, thus, a plausible explanation for the differences in the deformation mode at these latitudes (33–36° S).

## Conclusions

We present the first geodynamic models of intraplate lithospheric shortening for the Andes between 33° and 36° S. These models have allowed us to evaluate potential first-order and second-order controls on mountain building in this sector of the Andes. We tested the influence of the lithosphere–asthenosphere boundary (LAB) geometry, and the crustal thickness and composition over the deformation mode of the upper plate in a non-collisional orogen.

In all models, deformation took place where lithospheric thickness was smaller, indicating that the location of deformation is strongly controlled by lateral variations of this parameter. In addition, the geometry of the lithosphere–asthenosphere boundary (LAB) is a first-order control on deformation, especially with regard to the direction of tectonic transport within the orogen. The asymmetry of the LAB promotes west-dipping detachments and eastward propagation of faulting. We infer that this asymmetry is the result of corner flow associated with the east-dipping Nazca plate subducting beneath the South American continent.

Second-order controls are the initial thickness of the crust and lower-crustal composition. We observe that small crustal-thickness variations (~5 km) do not affect the deformation mode. However, the lower-crustal composition is an important factor controlling the deformation mode. A mafic and stronger lower crust produces a decoupled shortening mode of deformation, where lower- and upper-crustal deformation are offset towards the west or east, respectively. In contrast, a more felsic, and thus weaker, lower crust results in a coupled deformation mode. The former reproduces the conditions that cause deformation in the southern transect (36° S) and the latter represents the conditions in the northern transect (33° 40' S).

**Acknowledgments** This manuscript is a result of the PhD dissertation of M. Barrionuevo under a binational PhD program between the University of Buenos Aires (Argentina) and University of Potsdam (Germany). This research was supported by grants from CONICET (GII StRATEGy to L. Giambiagi), the Agencia de Promoción Científica y Tecnológica (PICT-2015-1181 to J.F. Mescua and PICT-2016-0269 to L. Giambiagi), and a grant by Deutsche Forschungsgemeinschaft (DFG) to M. Strecker (STR 373/34-1; StRATEGy). We are grateful to the editor U. Riller and the reviewers D. Whipp and J. Kley for their detailed reviews that significantly improved this manuscript. We thank Ch. Dullo, editor-in-chief, for handling this manuscript. We thank C. Kallich for support with artwork. We are grateful to have been able to use the Computational Infrastructure for Geodynamics (geodynamics.org), which is funded by the U.S. National Science Foundation under award EAR-0949446 and EAR-1550901, for supporting the development of ASPECT.

**Funding** This research was supported by grants from: CONICET (GII StRATEGy to L. Giambiagi) and the Agencia de Promoción Científica y Tecnológica (PICT-2015-1181 to J.F. Mescua and PICT-2016-0269 to L. Giambiagi); by the Deutsche Forschungsgemeinschaft and the Federal State of Brandenburg under the auspices of the International

Research Training Group IGK2018 “SuRfAce processes, TEctonics and Georesources: The Andean foreland basin of Argentina” (StRATEGy; DFG grant STR 373/34-1 to M.R. Strecker).

**Code availability** ASPECT is an open-source code hosted in Computational Infrastructure for Geodynamics (geodynamics.org).

## References

- Allmendinger RW, Gubbels T (1996) Pure and simple shear plateau uplift, Altiplano-Puna, Argentina and Bolivia. *Tectonophysics* 259:1–13. [https://doi.org/10.1016/0040-1951\(96\)00024-8](https://doi.org/10.1016/0040-1951(96)00024-8)
- Allmendinger RW, Ramos VA, Jordan TE et al (1983) Paleogeography and Andean structural geometry, northwest Argentina. *Tectonics* 2:1–16. <https://doi.org/10.1029/TC002i001p00001>
- Arcay D, Doin M-P, Tric E et al (2006) Overriding plate thinning in subduction zones: localized convection induced by slab dehydration. *Geochem Geophys Geosyst.* <https://doi.org/10.1029/2005GC001061>
- Armijo R, Rauld R, Thiele R et al (2010) The West Andean Thrust, the San Ramón Fault, and the seismic hazard for Santiago, Chile. *Tectonics.* <https://doi.org/10.1029/2008TC002427>
- Astaburuaga D (2014) Evolución estructural del límite Mesozoico-Cenozoico de la Cordillera Principal entre los 35 30' y 36 S, Región del Maule, Chile. Msc. Thesis. Dep. Geol. Univ. Chile, p 128
- Astini RA, Dávila FM (2010) Comment on “The West Andean Thrust, the San Ramón Fault, and the seismic hazard for Santiago, Chile” by Rolando Armijo et al. *Tectonics.* <https://doi.org/10.1029/2009TC002647>
- Astini RA, Benedetto JL, Vaccari NE (1995) The early Paleozoic evolution of the Argentine Precordillera as a Laurentian rifted, drifted, and collided terrane: a geodynamic model. *Geol Soc Am Bull* 107:253–273. [https://doi.org/10.1130/0016-7606\(1995\)107%3c0253:TEPEOT%3e2.3.CO;2](https://doi.org/10.1130/0016-7606(1995)107%3c0253:TEPEOT%3e2.3.CO;2)
- Azcuy CL, Caminos R (1987) Diastrofismo: El Sistema Carbonífero en la República Argentina. *Acad Nac Ciencias, Córdoba*, pp 239–252
- Babeyko AY, Sobolev SV (2005) Quantifying different modes of the late Cenozoic shortening in the central Andes. *Geology* 33:621–624. <https://doi.org/10.1130/G21126.1>
- Bangerth W, Dannberg J, Gassmüller R, Heister T (2018) ASPECT v2.0.1 [software]. <https://doi.org/10.5281/zenodo.1297145>
- Barrionuevo M (2020) The role of the upper plate in the Andean tectonic evolution (33–36°S): insights from structural geology and numerical modeling. Dissertation, University of Buenos Aires-University of Potsdam.
- Barrionuevo M, Giambiagi L, Mescua J et al (2019) Miocene deformation in the orogenic front of the Malargüe fold-and-thrust belt (35°30'–36° S): controls on the migration of magmatic and hydrocarbon fluids. *Tectonophysics.* <https://doi.org/10.1016/j.tecto.2019.06.005>
- Bastías-Mercado F, González J, Oliveros V (2020) Volumetric and compositional estimation of the Choiyoi Magmatic Province and its comparison with other Silicic Large Igneous Provinces. *J S Am Earth Sci* 102749
- Beaumont C, Ellis S, Hamilton J, Fullsack P (1996) Mechanical model for subduction-collision tectonics of Alpine-type compressional orogens. *Geology* 24:675. [https://doi.org/10.1130/0091-7613\(1996\)024%3c0675:MMFST%3e2.3.CO;2](https://doi.org/10.1130/0091-7613(1996)024%3c0675:MMFST%3e2.3.CO;2)
- Beaumont C, Nguyen M, Jamieson R, Ellis S (2006) Crustal flow modes in large hot orogens. In: Law RD, Searle MP, Godin L (eds) *Crustal flow, ductile extrusion and exhumation in*

- continental collision zones. *Geol. Soc. Spec. Publ.*, vol 268, pp 91–145
- Bookhagen B, Strecker MR (2012) Spatiotemporal trends in erosion rates across a pronounced rainfall gradient: examples from the southern Central Andes. *Earth Planet Sci Lett* 327–328:97–110. <https://doi.org/10.1016/j.epsl.2012.02.005>
- Boyce D, Charrier R, Farías M (2020) The first andean compressive tectonic phase: sedimentologic and structural analysis of mid-cretaceous deposits in the coastal cordillera, Central Chile (32°50'S). *Tectonics* 39:1–24. <https://doi.org/10.1029/2019TC005825>
- Brace WF, Kohlstedt DL (1980) Limits on lithospheric stress imposed by laboratory experiments. *J Geophys Res Solid Earth* 85:6248–6252. <https://doi.org/10.1029/jb085ib11p06248>
- Buelow EK, Suriano J, Mahoney JB et al (2018) Sedimentologic and stratigraphic evolution of the Cacheuta basin: constraints on the development of the Miocene retroarc foreland basin, south-central Andes. *Lithosphere*. <https://doi.org/10.1130/L709.1>
- Burov EB (2011) Rheology and strength of the lithosphere. *Mar Pet Geol* 28:1402–1443. <https://doi.org/10.1016/j.marpetgeo.2011.05.008>
- Burov EB, Watts AB (2006) The long-term strength of continental lithosphere: “jelly sandwich” or “crème brûlée”? *GSA Today* v. [https://doi.org/10.1130/1052-5173\(2006\)016%3c4:tltSOc%3e2.0.cO;2](https://doi.org/10.1130/1052-5173(2006)016%3c4:tltSOc%3e2.0.cO;2)
- Cahill T, Isacks BL (1992) Seismicity and shape of the subducted Nazca Plate. *J Geophys Res* 97:17503. <https://doi.org/10.1029/92JB00493>
- Cegarra MI, Ramos VA (1996) La faja plegada y corrida del Aconcagua. In: Ramos VA (ed) *Geología de la región del Aconcagua, Provincias de San Juan y Mendoza*, pp 387–422
- Charrier R, Baeza O, Elgueta S et al (2002) Evidence for Cenozoic extensional basin development and tectonic inversion south of the flat-slab segment, southern Central Andes, Chile (33°–36°S.L.). *J S Am Earth Sci* 15:117–139. [https://doi.org/10.1016/S0895-9811\(02\)00009-3](https://doi.org/10.1016/S0895-9811(02)00009-3)
- Charrier R, Ramos VA, Tapia F, Sagripanti L (2015) Tectono-stratigraphic evolution of the Andean Orogen between 31 and 37°S (Chile and Western Argentina). *Geol Soc Lond Spec Publ* 399:13–61. <https://doi.org/10.1144/sp399.20>
- Coutand I, Cobbold PR, De Urreiztieta M et al (2001) Style and history of Andean deformation, Puna plateau, northwestern Argentina. *Tectonics* 20:210–234. <https://doi.org/10.1029/2000TC900031>
- Currie CA, Beaumont C (2011) Are diamond-bearing Cretaceous kimberlites related to low-angle subduction beneath western North America? *Earth Planet Sci Lett* 303:59–70. <https://doi.org/10.1016/j.epsl.2010.12.036>
- Currie CA, Huismans RS, Beaumont C (2008) Thinning of continental backarc lithosphere by flow-induced gravitational instability. *Earth Planet Sci Lett* 269:436–447. <https://doi.org/10.1016/j.epsl.2008.02.037>
- Davis D, Dahlen FA, Suppe J (1983) Mechanics of fold-and-thrust belts and accretionary wedges Cohesive Coulomb theory. *J Geophys Res* 88:1153–1172. <https://doi.org/10.1029/JB089iB12p10087>
- Elger K, Oncken O, Glodny J (2005) Plateau-style accumulation of deformation: Southern Altiplano. *Tectonics* 24:1–19. <https://doi.org/10.1029/2004TC001675>
- Farías M, Comte D, Charrier R, Martinod J et al (2010) Crustal-scale structural architecture in central Chile based on seismicity and surface geology: implications for Andean mountain building. *Tectonics*. <https://doi.org/10.1029/2009TC002480>
- Fuentes F, Horton BK, Starck D, Boll A (2016) Structure and tectonic evolution of hybrid thick- and thin-skinned systems in the Malargüe fold-thrust belt, Neuquén basin, Argentina. *Geol Mag* 153:1066–1084. <https://doi.org/10.1017/S0016756816000583>
- Furlani R (2012) Tomografía de sismos locales en el retroarco andino centro-oeste Argentino entre 32°S y 33.5°S. Estructura cortical e implicaciones tectónicas. Phd Thesis. Universidad Nacional de San Juan
- Georgieva V, Gallagher K, Sobczyk A et al (2019) Effects of slab-window, alkaline volcanism, and glaciation on thermochronometer cooling histories, Patagonian Andes. *Earth Planet Sci Lett* 511:164–176. <https://doi.org/10.1016/j.epsl.2019.01.030>
- Gerbault M, Cembrano J, Mpodozis C et al (2009) Continental margin deformation along the Andean subduction zone: thermo-mechanical models. *Phys Earth Planet Inter* 177:180–205. <https://doi.org/10.1016/j.pepi.2009.09.001>
- Giambiagi LB, Ramos VA (2002) Structural evolution of the Andes in a transitional zone between flat and normal subduction (33 30'–33 45' S), Argentina and Chile. *J S Am Earth Sci* 15(1):101–116
- Giambiagi LB, Alvarez PP, Godoy E, Ramos VA (2003a) The control of pre-existing extensional structures on the evolution of the southern sector of the Aconcagua fold and thrust belt, southern Andes. *Tectonophysics* 369:1–19. [https://doi.org/10.1016/S0040-1951\(03\)00171-9](https://doi.org/10.1016/S0040-1951(03)00171-9)
- Giambiagi LB, Ramos VA, Godoy E et al (2003b) Cenozoic deformation and tectonic style of the Andes, between 33° and 34° south latitude. *Tectonics*. <https://doi.org/10.1029/2001TC001354>
- Giambiagi L, Mescua J, Bechis F, Tassara A, Hoke G (2012) Thrust belts of the southern Central Andes: along-strike variations in shortening, topography, crustal geometry, and denudation. *Bull Geol Soc Am* 124:1339–1351. <https://doi.org/10.1130/B30609.1>
- Giambiagi L, Tassara A, Mescua J et al (2015) Evolution of shallow and deep structures along the Maipo-Tunuyán transect (33°40'S): from the Pacific coast to the Andean foreland. *Geol Soc Lond Spec Publ* 399:63–82. <https://doi.org/10.1144/sp399.14>
- Gleason GC, Tullis J (1995) A flow law for dislocation creep of quartz aggregates determined with the molten salt cell. *Tectonophysics* 247:1–23. [https://doi.org/10.1016/0040-1951\(95\)00011-B](https://doi.org/10.1016/0040-1951(95)00011-B)
- Götze HJ, Meurers B, Schmidt S, Steinhäuser P (1991) On the isostatic state of the Eastern Alps and the Central Andes—a statistical comparison. *GSA Special Paper* 265:279–290
- Heister T, Dannberg J, Gassmüller R, Bangerth W (2017) High accuracy mantle convection simulation through modern numerical methods—II: realistic models and problems. *Geophys J Int* 210:833–851. <https://doi.org/10.1093/gji/ggx195>
- Hervé F, Demant A, Ramos VA, Pankhurst RJ, Suárez M (2000) The Southern Andes. *Tecton Evol South Am* 605–634
- Hilley GE, Strecker MR, Ramos VA (2004) Growth and erosion of fold-and-thrust belts with an application to the Aconcagua fold-and-thrust belt, Argentina. *J Geophys Res Solid Earth* 109:1–19. <https://doi.org/10.1029/2002JB002282>
- Hinojosa LF, Villagrán C (1997) Historia de los bosques del sur de Sudamérica, I: antecedentes paleobotánicos, geológicos y climáticos del Terciario del cono sur de América. *Rev Chil Hist Nat* 70:225–239
- Hirth G, Kohlstedt DL (2003) Rheology of the upper mantle and the mantle wedge: a view from the experimentalists. *Geophys Monogr Ser* 138:83–105. <https://doi.org/10.1029/138GM06>
- Hoke GD, Aranibar JN, Viale M et al (2013) Seasonal moisture sources and the isotopic composition of precipitation, rivers, and carbonates across the Andes at 32.5–35.5°S. *Geochem Geophys Geosyst* 14:962–978. <https://doi.org/10.1002/ggge.20045>
- Horton BK (2018) Tectonic regimes of the Central and Southern Andes: responses to variations in plate coupling during subduction. *Tectonics* 37:402–429. <https://doi.org/10.1002/2017TC004624>
- Horton BK, Fuentes F (2016) Sedimentary record of plate coupling and decoupling during growth of the Andes. *Geology* 44:647–650. <https://doi.org/10.1130/G37918.1>

- Horton BK, Fuentes F, Boll A et al (2016) Andean stratigraphic record of the transition from backarc extension to orogenic shortening: a case study from the northern Neuquén Basin, Argentina. *J S Am Earth Sci* 71:17–40. <https://doi.org/10.1016/j.jsame.2016.06.003>
- Ibarra F, Liu S, Meeßen C et al (2019) 3D data-derived lithospheric structure of the Central Andes and its implications for deformation: insights from gravity and geodynamic modelling. *Tectonophysics* 766:453–468. <https://doi.org/10.1016/j.tecto.2019.06.025>
- Irigoyen MV, Buchan KL, Brown RL (2000) Magnetostratigraphy of Neogene Andean foreland-basin strata, lat 33°S, Mendoza Province, Argentina. *Bull Geol Soc Am* 112:803–816. [https://doi.org/10.1130/0016-7606\(2000\)112%3c803:MONAF5%3e2.0.CO;2](https://doi.org/10.1130/0016-7606(2000)112%3c803:MONAF5%3e2.0.CO;2)
- Isacks BL (1988) Uplift of the Central Andean Plateau and bending of the Bolivian Orocline. *J Geophys Res* 93:3211. <https://doi.org/10.1029/JB093iB04p03211>
- Jackson J (2002) Strength of the continental lithosphere: time to abandon the jelly sandwich? *GSA Today* 12:4–10. [https://doi.org/10.1130/1052-5173\(2002\)012%3c0004:SOTCLT%3e2.0.CO;2](https://doi.org/10.1130/1052-5173(2002)012%3c0004:SOTCLT%3e2.0.CO;2)
- Jarrard RD (1986) Relations among subduction parameters. *Rev Geophys* 24:217–284
- Jordan TW, Isacks B, Allmendinger RW et al (1983) Andean tectonics related to geometry of subducted Nazca plate. *Geol Soc Am Bull* 94:341. [https://doi.org/10.1130/0016-7606\(1983\)94%3c341:ARTGO%3e2.0.CO;2](https://doi.org/10.1130/0016-7606(1983)94%3c341:ARTGO%3e2.0.CO;2)
- Julve J (2019) Estructura cortical bajo los Andes del Sur y rol del régimen termo-mecánico en la distribución y estilo de su deformación. Memoria para optar al Título de Geólogo. <http://repositorio.udec.cl/jspui/handle/11594/3443>
- Kay SM, Mpodozis C (2002) Magmatism as a probe to the Neogene shallowing of the Nazca plate beneath the modern Chilean flat-slabs. *J S Am Earth Sci* 15:39–57. [https://doi.org/10.1016/S0895-9811\(02\)00005-6](https://doi.org/10.1016/S0895-9811(02)00005-6)
- Kay SM, Ramos VA, Mpodozis C, Sruoga P (1989) Late Paleozoic to Jurassic silicic magmatism at the Gondwana margin: analogy to the Middle Proterozoic in North America? *Geology* 17:324–328. [https://doi.org/10.1130/0091-7613\(1989\)017%3c0324:LPTJSM%3e2.3.CO;2](https://doi.org/10.1130/0091-7613(1989)017%3c0324:LPTJSM%3e2.3.CO;2)
- Kay SM, Godoy E, Kurtz A (2005) Episodic arc migration, crustal thickening, subduction erosion, and magmatism in the south-central Andes. *Bull Geol Soc Am* 117:67–88. <https://doi.org/10.1130/B25431.1>
- Kay SM, Burns WM, Copeland P, Mancilla O (2006) Upper Cretaceous to Holocene magmatism and evidence for transient Miocene shallowing of the Andean subduction zone under the northern Neuquén Basin. *Spec Pap Soc Am* 407:19
- Kimbrough DL, Mahoney JB, Mescua JF, Giambiagi LB, Buelow EK (2015) New zircon U-Pb ages define a strongly episodic history of magmatism for the Permo-Triassic Choiyoi Silicic Large Igneous Province of Chile and Argentina. In: Geological Society of America Annual Meeting 2015, conference proceedings. *GSA Abstracts with Programs*, vol 47, no 7, Paper 196-9
- Kleiman LE, Japas MS (2009) The Choiyoi volcanic province at 34 S–36 S (San Rafael, Mendoza, Argentina): implications for the Late Palaeozoic evolution of the southwestern margin of Gondwana. *Tectonophysics* 473(3–4):283–299
- Kley J, Monaldi CR, Salfity JA (1999) Along-strike segmentation of the Andean foreland: causes and consequences. *Tectonophysics* 301:75–94. [https://doi.org/10.1016/S0040-1951\(98\)90223-2](https://doi.org/10.1016/S0040-1951(98)90223-2)
- Kozlowski E, Manceda R, Ramos VA (1993) Estructura. In: *Geología y recursos naturales de Mendoza*. Asociación Geológica, Buenos Aires, pp 235–256
- Kronbichler M, Heister T, Bangerth W (2012) High accuracy mantle convection simulation through modern numerical methods. *Geophys J Int* 191:12–29. <https://doi.org/10.1111/j.1365-246X.2012.05609.x>
- Kusznrir NJ, Park RG (1986) Continental lithosphere strength: the critical role of lower crustal deformation. *Geol Soc Lond Spec Publ* 24:79–93. <https://doi.org/10.1144/gsl.sp.1986.024.01.09>
- Kusznrir NJ, Whitmarsh RB, England P et al (1991) The distribution of stress with depth in the lithosphere: thermo-rheological and geodynamic constraints [and Discussion]. <https://doi.org/10.1098/rsta.1991.0109>
- Lacombe O, Bellahsen N (2016) Thick-skinned tectonics and basement-involved fold–thrust belts: insights from selected Cenozoic orogens. *Geol Mag* 153:763–810. <https://doi.org/10.1017/S0016756816000078>
- Litvak VD et al (2018) The Late Paleogene to Neogene Volcanic Arc in the Southern Central Andes (28°–37° S). In: Folguera A et al (eds) *The evolution of the Chilean-Argentinean Andes*. Springer Earth System Sciences. Springer, Cham. [https://doi.org/10.1007/978-3-319-67774-3\\_20](https://doi.org/10.1007/978-3-319-67774-3_20)
- Liu S (2020) Controls of foreland-deformation patterns in the orogen-foreland shortening system. PhD thesis, University of Potsdam, Potsdam
- Liu S, Currie CA (2016) Farallon plate dynamics prior to the Laramide orogeny: numerical models of flat subduction. *Tectonophysics* 666:33–47. <https://doi.org/10.1016/j.tecto.2015.10.010>
- Llambías EJ, Kleiman LE, Salvarredi JA (1993) El magmatismo gondwánico. In: Ramos V (ed) *Geología y Recursos Naturales de Mendoza*. Congreso Geológico Argentino, pp 53–64
- Lossada AC, Hoke GD, Giambiagi LB et al (2020) Detrital thermochronology reveals major middle Miocene exhumation of the eastern flank of the Andes that predates the Pampean flat-slab (33°–33.5°S). *Tectonics*. <https://doi.org/10.1029/2019tc005764>
- Lowry AR, Pérez-Gussinyé M (2011) The role of crustal quartz in controlling Cordilleran deformation. *Nature* 471:353–359. <https://doi.org/10.1038/nature09912>
- Lucazeau F (2019) Analysis and mapping of an updated terrestrial heat flow data set. *Geochem Geophys Geosyst* 20:4001–4024. <https://doi.org/10.1029/2019GC008389>
- Mackwell SJ, Zimmerman ME, Kohlstedt DL (1998) High-temperature deformation of dry diabase with application to tectonics on Venus. *J Geophys Res Solid Earth* 103:975–984. <https://doi.org/10.1029/97jb02671>
- Macpherson CG (2008) Lithosphere erosion and crustal growth in subduction zones: insights from initiation of the nascent East Philippine Arc. *Geology* 36:311–314. <https://doi.org/10.1130/G24412A.1>
- Manceda R, Figueroa D (1995) Inversion of the Mesozoic Neuquén Rift in the Malargue fold and thrust belt, Mendoza, Argentina. In: Tankard AJ, Suarez RS, Welsink HJ (eds) *Pet basins South Am AAPG Mem*, vol 62, pp 369–382
- Marot M, Monfret T, Gerbault M et al (2014) Flat versus normal subduction zones: a comparison based on 3-D regional traveltimes tomography and petrological modelling of central Chile and western Argentina (29°–35°S). *Geophys J Int* 199:1633–1654. <https://doi.org/10.1093/gji/ggu355>
- Massonne HJ, Calderón M (2008) P-T evolution of metapelites from the Guarguaraz Complex, Argentina: evidence for Devonian crustal thickening close to the western Gondwana margin. *Rev Geol Chile* 35:215–231. <https://doi.org/10.4067/S0716-02082008000200002>
- McGroder MF, Lease RO, Pearson DM (2015) Along-strike variation in structural styles and hydrocarbon occurrences, Subandean fold-and-thrust belt and inner foreland, Colombia to Argentina. In: *Geodynamics of a cordilleran orogenic system: the Central*

- Andes of Argentina and Northern Chile. Geological Society of America, p 2016. [https://doi.org/10.1130/2015.1212\(05\)](https://doi.org/10.1130/2015.1212(05))
- Meeßen C, Sippel J, Scheck-Wenderoth M et al (2018) Crustal structure of the Andean Foreland in Northern Argentina: results from data-integrative three-dimensional density modeling. *J Geophys Res Solid Earth* 123:1875–1903. <https://doi.org/10.1002/2017JB014296>
- Mescua JF, Giambiagi LB, Ramos VA (2013) Levantamiento cretácico tardío en la faja plegada y corrida de malargüe (35°S), Andes Centrales del sur, Argentina y Chile. *Andean Geol* 40:102–116. <https://doi.org/10.5027/andgeoV40n1-a05>
- Mescua JF, Giambiagi LB, Tassara A et al (2014) Influence of pre-Andean history over Cenozoic foreland deformation: Structural styles in the Malargüe fold-and-thrust belt at 35°S, Andes of Argentina. *Geosphere* 10:585–609. <https://doi.org/10.1130/GES00939.1>
- Mescua JF, Giambiagi L, Barrionuevo M et al (2016) Basement composition and basin geometry controls on upper-crustal deformation in the Southern Central Andes (30–36°S). *Geol Mag* 153:945–961. <https://doi.org/10.1017/S0016756816000364>
- Mouthereau F, Watts AB, Burrov E (2013) Structure of orogenic belts controlled by lithosphere age. *Nat Geosci* 6:785–789. <https://doi.org/10.1038/ngeo1902>
- Mpodozis C, Cornejo P (2012) Cenozoic Tectonics and Porphyry Copper Systems of the Chilean Andes. *Geology and genesis of major copper deposits and districts of the world: a tribute to Richard H. Sillitoe*. Soc Econ Geol, Boulder, pp 329–360
- Mpodozis C, Ramos VA (1989) The Andes of Chile and Argentina. In: *Geology of the Andes and its relation to hydrocarbon and mineral resources*, vol 11. Circumpacific Counc Energy Miner Resour, pp 59–90
- Nyström J, Vergara M, Morata D, Levi B (2003) Tertiary volcanism during extension in the Andean foothills of central Chile (33°15′–33°45′S). *Geol Soc Am Bull* 115:1523. <https://doi.org/10.1130/B25099.1>
- Oliveros V, González J, Espinoza Vargas M et al (2018) The early stages of the magmatic arc in the Southern Central Andes, pp 165–190
- Oncken O, Hindle D, Kley J, Elger K, Victor P, Schemmann K (2006) Deformation of the Central Andean Upper Plate System—facts, fiction, and constraints for plateau models. In: *The Andes*. Springer, Berlin, pp 3–27. [https://doi.org/10.1007/978-3-540-48684-8\\_1](https://doi.org/10.1007/978-3-540-48684-8_1)
- Orts DL, Folguera A, Giménez M, Ramos V (2012) Variable structural controls through time in the Southern Central Andes (~36°S). *Andean Geol* 39:220–241. <https://doi.org/10.5027/andgeoV39n2-a02>
- Peacock SA (1990) Fluid processes in subduction zones. *Science* 80(248):329–337. <https://doi.org/10.1126/science.248.4953.329>
- Pearson DM, Kapp P, DeCelles PG, Reiners PW, Gehrels GE, Ducea MN, Pullen A (2013) Influence of pre-Andean crustal structure on Cenozoic thrust belt kinematics and shortening magnitude: Northwestern Argentina. *Geosphere* 9:1766–1782. <https://doi.org/10.1130/GES00923.1>
- Piquer J, Rivera O, Yañez G, Oyarzun N (2020) The Piuquencillo Fault System: a long-lived, Andean-transverse fault system and its relationship with magmatic and hydrothermal activity. *Solid Earth Discuss*. <https://doi.org/10.5194/se-2020-142>
- Ramos VA (1988) The tectonics of the Central Andes; 30° to 33° S latitude. In: Clark Jr SP, Burchfiel BC, Suppe J (eds) *Processes in Continental Lithospheric Deformation*. Geological Society of America. <https://doi.org/10.1130/SPE218-p31>
- Ramos VA (1999) Plate tectonic setting of the Andean Cordillera. *Episodes* 22:183–190. <https://doi.org/10.1111/lj.1365-2621.2006.01230.x>
- Ramos VA (2010) The tectonic regime along the Andes: present-day and Mesozoic regimes. *Geol J* 45:2–25. <https://doi.org/10.1002/gj.1193>
- Ramos VA, Folguera A (2011) Payenia volcanic province in the Southern Andes: an appraisal of an exceptional quaternary tectonic setting. *J Volcanol Geotherm Res* 201:53–64. <https://doi.org/10.1016/j.jvolgeores.2010.09.008>
- Ramos VA, Jordan TE, Allmendinger RW et al (1986) Paleozoic terranes of the central Argentine-Chilean Andes. *Tectonics* 5:855–880. <https://doi.org/10.1029/TC005i006p00855>
- Ramos VA, Cegarra M, Cristallini E (1996) Cenozoic tectonics of the High Andes of west-central Argentina (30–36°S latitude). *Tectonophysics* 259:185–200. [https://doi.org/10.1016/0040-1951\(95\)00064-X](https://doi.org/10.1016/0040-1951(95)00064-X)
- Ramos VA, Cristallini EO, Pérez DJ (2002) The Pampean flat-slab of the Central Andes. *J S Am Earth Sci* 15:59–78. [https://doi.org/10.1016/S0895-9811\(02\)00006-8](https://doi.org/10.1016/S0895-9811(02)00006-8)
- Ramos VA, Zapata T, Cristallini EO, Introcaso A (2004) The Andean thrust system—latitudinal variations in structural styles and orogenic shortening. *AAPG Mem* 82:30–50
- Ranalli G, Murphy DC (1987) Rheological stratification of the lithosphere. *Tectonophysics* 132:281–295. [https://doi.org/10.1016/0040-1951\(87\)90348-9](https://doi.org/10.1016/0040-1951(87)90348-9)
- Riesner M, Lacassin R, Simoes M et al (2018) Revisiting the crustal structure and kinematics of the Central Andes at 33.5°S: implications for the mechanics of Andean mountain building. *Tectonics* 37:1347–1375. <https://doi.org/10.1002/2017TC004513>
- Rodríguez Picada C, Scheck Wenderoth M, Gomez Dacal ML et al (2020) Lithospheric density structure of the southern Central Andes constrained by 3D data-integrative gravity modelling. *Int J Earth Sci*. <https://doi.org/10.1007/s00531-020-01962-1>
- Sato AM, Llambías EJ, Basei MAS, Castro CE (2015) Three stages in the Late Paleozoic to Triassic magmatism of southwestern Gondwana, and the relationships with the volcanogenic events in coeval basins. *J S Am Earth Sci* 63:48–69. <https://doi.org/10.1016/j.jsames.2015.07.005>
- Schellart WP (2004) Kinematics of subduction and subduction-induced flow in the upper mantle. *J Geophys Res Solid Earth* 109:1–19. <https://doi.org/10.1029/2004JB002970>
- Scheuber E et al (2006) Exhumation and basin development related to formation of the Central Andean Plateau, 21° S. In: Oncken O et al (eds) *The Andes*. *Frontiers in Earth Sciences*. Springer, Berlin. [https://doi.org/10.1007/978-3-540-48684-8\\_13](https://doi.org/10.1007/978-3-540-48684-8_13)
- Schmelting H, Babeyko AY, Enns A et al (2008) A benchmark comparison of spontaneous subduction models. Towards a free surface. *Phys Earth Planet Inter* 171:198–223. <https://doi.org/10.1016/j.pepi.2008.06.028>
- SEGEMAR (1997) Mapa Geológico de la República Argentina, Escala 1:2.500.000. Servicio Geológico y Minero Argentino
- SERNAGEOMIN (2003) Mapa Geológico de Chile, Escala 1:1.000.000. Servicio Nacional de Geología y Minería, Publicación Geológica Digital no. 4
- Sigismondi ME (2012) Estudio de la deformación litosférica de la cuenca Neuquina: estructura termal, datos de gravedad y sísmica de reflexión. Dissertation. University of Buenos Aires
- Silvestro J, Kraemer P, Achilli F, Brinkworth W (2005) Evolución de las cuencas sinorogénicas de la Cordillera Principal entre 35–36° S, Malargüe. *Rev la Asoc Geol Argentina* 60:627–643
- Sobolev SV, Babeyko AY (2005) What drives orogeny in the Andes? *Geology* 33:617–620. <https://doi.org/10.1130/G21557.1>
- Sobolev SV, Babeyko AY, Koulakov I, Oncken O (2006) Mechanism of the Andean orogeny: insight from numerical modeling. In: *The Andes*. Springer, pp 513–535
- Somoza R, Ghidella ME (2012) Late Cretaceous to recent plate motions in western South America revisited. *Earth Planet Sci Lett* 331–332:152–163. <https://doi.org/10.1016/j.epsl.2012.03.003>

- Sruoga P, Rubinstein NA, Etcheverría MP et al (2008) Estadío inicial del arco volcánico Neógeno en la Cordillera principal de Mendoza (35° S). *Rev la Asoc Geol Argentina* 63:454–469
- Stalder NF, Herman F, Fellin GM et al (2020) The relationships between tectonics, climate and exhumation in the Central Andes (18–36°S): evidence from low-temperature thermochronology. *Earth Sci Rev*. <https://doi.org/10.1016/j.earscirev.2020.103276>
- Stern CR, Skewes MA (1995) Miocene to present magmatic evolution at the northern end of the Andean Southern Volcanic Zone, Central Chile. *Andean Geol* 22:261–272. <https://doi.org/10.5027/ANDGEOV22N2-A09>
- Strecker MR, Alonso RN, Bookhagen B et al (2007) Tectonics and climate of the Southern Central Andes. *Annu Rev Earth Planet Sci* 35:747–787. <https://doi.org/10.1146/annurev.earth.35.031306.140158>
- Tapia F (2015) Evolución Tectónica y Configuración Actual De Los Andes Centrales del Sur (34°46'–35°30'S). Dissertation. Universidad de Chile
- Tassara A, Echaurren A (2012) Anatomy of the Andean subduction zone: three-dimensional density model upgraded and compared against global-scale models. *Geophys J Int* 189:161–168. <https://doi.org/10.1111/j.1365-246X.2012.05397.x>
- Tassara A, Yáñez G (2003) Relación entre el espesor elástico de la litosfera y la segmentación tectónica del margen andino (15–47°S). *Rev Geol Chile* 30:1–35. <https://doi.org/10.4067/S0716-02082003000200002>
- Tassara A, Götze HJ, Schmidt S, Hackney R (2006) Three-dimensional density model of the Nazca plate and the Andean continental margin. *J Geophys Res Solid Earth* 111:1–26. <https://doi.org/10.1029/2005JB003976>
- Thomson SN, Brandon MT, Tomkin JH et al (2010) Glaciation as a destructive and constructive control on mountain building. *Nature* 467:313–317. <https://doi.org/10.1038/nature09365>
- Tunik M, Folguera A, Naipauer M et al (2010) Early uplift and orogenic deformation in the Neuquén Basin: constraints on the Andean uplift from U-Pb and Hf isotopic data of detrital zircons. *Tectonophysics* 489:258–273. <https://doi.org/10.1016/j.tecto.2010.04.017>
- Turienzo M, Dimieri L, Frisicale C, Araujo V, Sánchez N (2012) Cenozoic structural evolution of the Argentinean Andes at 34°40'S: a close relationship between thick and thin-skinned deformation. *Andean Geol*. <https://doi.org/10.5027/andgeoV39n2-a07>
- Uliana MA, Biddle KT, Cerdan J (1989) Mesozoic extension and the formation of Argentine sedimentary basins: chapter 39: analogs
- Val P, Venerdini AL, Ouimet W et al (2018) Tectonic control of erosion in the southern Central Andes. *Earth Planet Sci Lett* 482:160–170. <https://doi.org/10.1016/j.epsl.2017.11.004>
- Vergani GD, Tankard AJ, Belotti HJ, Welsink HJ (1995) Tectonic evolution and paleogeography of the Neuquen Basin, Argentina: abstract. In: AAPG bulletin. AAPG Special Volumes, pp 383–402
- Vilà M, Fernández M, Jiménez-Munt I (2010) Radiogenic heat production variability of some common lithological groups and its significance to lithospheric thermal modeling. *Tectonophysics* 490:152–164. <https://doi.org/10.1016/j.tecto.2010.05.003>
- Willett SD (1999) Orogeny and orography: the effects of erosion on the structure of mountain belts. *J Geophys Res Solid Earth* 104:28957–28981. <https://doi.org/10.1029/1999jb900248>
- Wolf SG, Huismans RS (2019) Mountain building or backarc extension in ocean-continent subduction systems—a function of backarc lithospheric strength and absolute plate velocities. *J Geophys Res Solid Earth*. <https://doi.org/10.1029/2018JB017171>
- Yáñez G, Cembrano J (2004) Role of viscous plate coupling in the late Tertiary Andean tectonics. *J Geophys Res Solid Earth* 109:1–21. <https://doi.org/10.1029/2003jb002494>
- Yáñez GA, Gana P, Fernández R (1998) Origen y significado geológico de la Anomalía Melipilla. *Chile Central Rev Geol Chile*. <https://doi.org/10.4067/S0716-02081998000200005>